의학박사 학위논문

Tissue Regeneration effects of 3D-Printed Antibiotic-Releasing Esophageal Patches

3D 프린팅을 이용한 항생제 방출 식도 패치의 조직 재생 효과에 대한 연구

2021년 8월

서울대학교 대학원

의학과 이비인후과학 전공

김 성 동

Tissue Regeneration effects of 3D-Printed Antibiotic-Releasing Esophageal Patches

지도 교수 정 은 재

이 논문을 의학박사 학위논문으로 제출함
2021년 4월

서울대학교 대학원
의학과 이비인후과학 전공
김 성 동

김성동의 의학박사 학위논문을 인준함
2021년 7월

위 원 장 안 순 현

부위원장 정 은 재

위 원 박 인 규

위 원 박 무 균

위 원 임 윤 성

Abstract

Esophageal defects can cause exposure of the fistula site to various bacterial species, which could lead to a severe inflammatory response. We designed and manufactured a 3D-printed patch consisting of a lattice pattern and thin-film with biodegradable polycaprolactone (PCL), that released the antibiotic, tetracycline (TCN). We reconstructed an artificial defect in the rat esophagus using this patch. The efficacy and availability of 3D-printed antibiotic-releasing patches were evaluated using both quantitative and qualitative assessment methods.

PCL was used to print the lattice pattern on a pre-manufactured thin film with approximately 100μm resolution, which had been mixed with tetracycline (TCN) at 100° C and 1000° C to release the antibiotic evenly. *In vitro* tests showed that TCN was released for more than 1 month. In addition, *in vitro* cytotoxicity test demonstrated excellent cell compatibility. 3D-printed antibiotic-releasing patches were applied on the defect sites after creating artificial partial esophageal defects in rats. Four weeks after the surgery, leakage was checked using micro-computed tomography with an oral contrast agent injected into the rat mouth. No leakage was evident in any part of the esophagus. For analyzing tissue regeneration, immunohistochemistry was performed. M1 and M2 macrophage activation was verified by immunohistochemistry of CD-68 and CD-163. Desmin immunohistochemistry showed significant muscle layer regeneration in the TCN (1% and 3%) patch groups. Moreover, sufficient re-epithelialization and neo-vascularization were affirmed in TCN (1% and 3%) patch groups.

In this study, we confirmed that 3D-printed antibiotic-releasing patches not only have anti-microbial effects but also have tissue regeneration ability in the area surrounding the esophageal fistula site. The results of this study can be applied in further studies on tissue-engineering.

Key Words : Esophagus, Reconstruction, Tissue-engineering, Surgical Patch, Antibiotic-releasing patch

Student Number : 2018-31720

Table of Contents

Chapter 1. Introduction

1.1. Study Background

The upper digestive tract is a hollow organ and consists of the mouth, pharynx, esophagus, stomach, and duodenum. The lumen of the upper digestive tract is a contaminated space comprising diverse normal flora and food components. Especially, the pharynx and esophagus are the sites of the beginning of the food pathway. Hence, they are exposed to food and bacteria that are not treated by sufficient digestion or sterilization. The presence of defects in the pharynx or esophagus can leak these contaminants causing infection or inflammation.[1] Once leakage occurs, the defect site can increase in size because of the weakening of the pharyngeal or esophageal wall. Additionally, if such defects involve important anatomic structures such as major vessels including carotid artery and jugular vein, severe bleeding or sepsis may occur, which can be fatal. [2, 3]

Such defects may be caused by esophageal or pharyngeal cancers, surgery for cancer, trachea–esophageal fistula, and traumatic insults. Among these conditions, defect formation after cancer surgery is most common to a surgeon, and broadly two repairing methods have been proposed for that. The first is primary suturing, which can be applied when the defect site can be closely approximated, and the other is autogenous tissue transplantation, which is used when the defect size is large.[4] Currently used operation techniques of autogenous tissue transplantation for

pharyngoesophageal defects are radial forearm free flap, anterolateral thigh free flap, gastric pull-up flap, jejunal free flap, and colon interposition flaps [5-7].

However, autogenous transplantation requires longer operation times and is associated with donor site morbidity.[4, 8-10] Thus, alternative strategies are sought.[11, 12] One is the synthetic polymer patch. Commercial surgical patches are designed for clean wounds such as those of the blood vessels, abdominal wall, or dura. However, the digestive tract is continuously exposed to contaminants. Accordingly, the application of existing surgical patches can cause weakness of the anastomosis site and eventually result in leakage after some time. Therefore, the patch should induce rapid tissue regeneration and have durability against contaminants. However, no such commercial patch is available right now.

1.2. Purpose of Research

We affiliated with Dr. Noh's team at Seoul National University of Science and Technology who developed a precise manufacturing technique for diverse bio-gradable materials using three-dimensional (3D) printing. [13, 14] We designed 3D printed patch for the contaminated environment of the esophagus lumen by application of our experience from the previous esophageal reconstruction study using polyurethane artificial esophagus. [15] The framework of this patch was fabricated using bio-degradable polycaprolactone (PCL). A 3D-printed multi-layer lattice structure was designed for bearing the shear stresses of esophageal peristalsis, and a thin PCL film was incorporated in the center of the patch to overcome the limitation of the porous structure of the patch due to the presence of the lattice. A lattice structure with pores was designed for the penetration of neo-generated muscles and blood vessels. Moreover, antibiotics such as tetracycline (TCN) were incorporated in the patch, designed to be released slowly at the implanted site. The study was designed to evaluate the effect of different concentrations of antibiotics. This antibiotic-releasing patch was applied to an artificial defect created in the rat esophagus and micro-anastomosis was performed to cover the defect.

Therefore, the purpose of this study was to analyze and discuss the antibiotic-releasing ability and role in tissue regeneration of a 3D-printed antibiotic-releasing patch through implantation in a partially defective rat esophagus.

Chapter 2. Materials and methods

2.1. Outline of the study

First, a 3D-printed PCL patch was designed. Simultaneously, experimental rats underwent surgery for creating a fistula. Bacterial species from the defect site were cultured and an antibiotic sensitivity test was performed. Accordingly, the most effective antibiotics were determined. Thereafter, these antibiotics were loaded in the PCL patch, and the antibiotic-releasing behavior was analyzed. After testing the cytotoxicity of the designed patch, the patch was implanted in all rats. Then several tests were performed in the sacrificed rats in each group at the end of 4 weeks and 12 weeks, postoperatively.

A micro-computed tomography (μCT) scan with peroral contrast was performed to assess the leakage status from the defect after patch implantation. A tissue specimen from the patched site was collected, and hematoxylin and eosin (H&E) staining and immunohistochemical analysis including desmin and elastin was performed to analyze the extent of tissue regeneration. Figure 1 shows the flow chart of the outline.

2.2. Manufacture of the antibiotic-releasing patch

1) Patch design

The patch was designed as a lattice structure (1 cm × 1 cm) using the SolidWorks software (Dassault Systems, SolidWorks Corp, Waltham, USA). The designed files were exported in the standard tessellation language format to a 3D printing software (Simplify 3D Version 4.0, Cincinnati, Ohio, USA) to generate G-code commands. A homemade 3D printer was used as a deposition system to fabricate the lattice pattern, as described previously[13]. Tetracycline (TCN) and polycaprolactone (PCL, MW = 80000) were purchased from Sigma-Aldrich (St. Louis, MO, USA). The PCL pellets were heated at 100° C for approximately 25 minutes to melt them completely. TCN powders in predetermined concentrations were mixed into the molten polymeric material using a sonicator at 1000° C for 5 minutes. The PCL+TCN mixture was loaded in the stainless-steel syringe (Musashi Engineering, Mitaka-shi, Tokyo, Japan) of the in-house extrusion 3D printer.

The PCL 3D printing process was as follows:

1. A PCL film was prepared by dissolving 1 g of PCL pellets in 10 ml of acetone for 4 hours at 300 rpm. The solution was cast on a Teflon sheet in a polystyrene petri dish (d = 10 cm) and kept under a vacuum for 3 days to ensure the complete removal of the solvents. The PCL film was then packed into the substrate.

2. The TCN-loaded PCL solution was pneumatically printed in a lattice structure using a needle at 720kPa and printing velocity of 12 mm per minute on the thin PCL film.

The fabrication steps 1 and 2 were repeated until TCN-loaded PCL printing patches with 4 layers in the lattice form were obtained.

2) Physio-chemical characteristics of the 3D-printed patches

After fabrication, the surface and cross-section morphologies of the 3D-printed patches were observed using a scanning electron microscope (SEM; TESCAN VEGA 3, Tescan Orsay Holdings, Kohoutovice, Czech Republic). The PCL patches were platinum-coated using a sputter-coater, and the morphologies were acquired at an accelerating voltage of 15kV.

A tensile test was conducted to measure the mechanical strength of the 3D-printed patches, All test specimens were designed according to the ISO 527-1 standards, the printed specimens with rectangular shapes (10 mm × 50 mm × 0.2 mm) in a lattice structure were prepared.

Three groups of specimens were prepared for comparative analysis:

1. PCL lattice without film
2. PCL lattice with film
3. TCN-loaded PCL patch (1mg/g of specimen) with PCL film

A micro-fatigue tester (E3000LT, INSTRON, UK) was used for performing measurements. Briefly, the specimens were gripped at 20 mm from each edge and stretched at a strain rate of 2 mm/min (n=3 per group), The shear stress over the shear rate of the test

was measured until breakage.

The antibiotic-releasing kinetics of the patch were assessed by immersing the printed patches in 10 ml phosphate-buffered saline (PBS) at 37° C (n=3 per condition). A 100 μL aliquot from all released media was collected and replaced with the same amount of fresh PBS at defined intervals (1, 3, 6, and 12 hours and 1, 3, 5, 10, 15, 20, 25, and 30 days). The concentration of TCN in the released media was calculated by using a UV-VIS spectrophotometer (BioMate 3S, Thermo Fisher Scientific, Waltham, MA, USA)

3) In vitro cytotoxicity test of patches

The *in vitro* cytotoxicity of the 3D-printed PCL/TCN patches was analyzed using a previously described protocol.[14] Teflon, latex, and 3D-printed patches were cut in round shapes with 1 cm diameter. Then, 1.2 mL of α-MEM media containing 10% fetal bovine serum and 1% penicillin-streptomycin was added to a 24-well plate for three-day incubation.

In addition, 1×10^4 osteoblast cells derived from Mus musculus mice (MC3T3, Sigma-Aldrich) were seeded in a 96-well plate with α-MEM media in the incubator (37° C, 5% CO_2) for one day. Osteoblast cell (MC3T3) was selected based on the experience from the previous study.[16] The medium in each well was replaced with 100 μL of extract solution from the prepared samples for another one-day incubation. Next, thiazolyl blue tetrazolium bromide (MTT), bromodeoxyuridine (BrdU), and neutral red solutions were added, and samples were further incubated for 4

hours. MTT, neutral red, and BrdU assays were used to determine the cytotoxicity of the samples for micro-organs such as mitochondria, lysosomes, and DNA, respectively. Teflon and latex were used as positive and negative controls respectively. Finally, the optical densities of the samples were determined by a microplate reader (Tecan GENios, GMI, Minnesota, USA) at a wavelength of 570 nm.

The cell viability of the above samples was determined as per the protocol published in a previous paper.[15] In this assay, 1×10^5 MC3T3 cells were seeded on each test sample. Live and dead cell images from the prepared samples were acquired for extractions after 3 days under a fluorescence inverted microscope (Leica Microsystems, Wetzlar, Germany).

2.2. Animal Study

1) Culture and anti-microbial susceptibility test

Adult Sprague-Dawley rats (Orient Bio, Seoul, Korea) that weighed 398 to 420g were used for microbiological culture and esophageal transplantation. Rats in which artificial fistulas were created were sacrificed by Day 3 to assess the bacterial flora. We opened the wound and performed swab culture at the fistula site. Swabs with the bacteria were inoculated on a plate with a bacterial growth medium (Gibco LB broth, Thermo Fisher Scientific). The bacterial flora extracted from each esophageal fistula model was grown for 3 days and then subjected to an antimicrobial susceptibility test (AST-P601 card; bioMerieux, Marcy l'Etoile, France). When the rats in the patched groups were sacrificed, swab culture was performed on the samples obtained from the outside of the patch or regenerated tissue.

2) Grouping, surgical technique, and postoperative management

We formed the following five groups for analyzing the effect of each patch according to the concentration of antibiotics:

Group 1. Defect only (Control, N=10)

Group 2. Implantation of patch without TCN
[TCN (w/o) patch, N=6]

Group 3. Implantation of patch with 0.3mg of TCN
[TCN (0.3%) patch, N=6]

Group 4. Implantation of patch with 1.0 mg of TCN
[TCN (1%) patch, N=6]

Group 5. Implantation of patch with 2.5 mg of TCN
[TCN (3%) patch, N=6]

The surgical procedure for all rats was as follows:

Under sedation, the necks of all rats were shaved. Routine scrubbing using betadine was performed for ensuring an aseptic environment. A vertical midline incision in the neck was made from the level of the hyoid bone to the jugular notch. After separating the strap muscles, the thyroid isthmus was cut, and the trachea was exposed. In the left-posterior site of the trachea, we identified the esophagus and created a partial esophageal defect (120° partial circumferential defect). We repaired the artificial esophageal fistulas using 3D-printed patches, as shown in Figure 2 (8-way stitch with 8-0 vicryl sutures under a microscope), in rats of Groups 2-5. Then, vertical matrix-type skin suturing was performed using 5-0 nylon sutures. All animals were housed in

individual metabolic cages obtained from our animal facility.

Postoperative monitoring, such as animal survival and weight, was performed every day. In addition, the experimental rats were examined according to previously described indicators of appearance and behavior on a 5-point scale (Table 1) [17]

This study was performed in strict accordance with the guidelines of the Animal Research Committee, Seoul National University Hospital. All protocols and experimental design parameters were reviewed and approved by the Institutional Animal Care and Use Committee of the Seoul National University Hospital (Approval number: 17-0164-S1A0).

2.3. Radiological examination

A μCT scanner (NFR Polaris-G90, Nanofocusray, Korea) was used to assess the leakage of saliva from the esophageal defect. Before the CT scan, all rats were orally injected with barium sulfate (Solotop HD, Taejoon Pharm. Co. Ltd., Seoul, South Korea), a contrast agent. Then 3D images of the rat esophagus were obtained and reconstructed using a software program (Lucion, Infinitt Healthcare, Korea). All experimental rats were sacrificed after the radiological examination.

2.4. Histological examination

A specimen of the esophageal tissue with the implanted patch was obtained from the patch site, and each specimen was fixed in 10% neutral-buffered formalin, embedded in paraffin, and cut in sections of 4-μm thickness. The sections were deparaffinized and dehydrated in graded series of ethanol. The tissue slides were then stained with hematoxylin and eosin (H&E) and Masson's trichrome following standard histological procedures. Elastin staining was also performed according to the manufacturer's instructions using an elastic (modified Verhoff's) stain kit (ES4807). All histological images were captured using a light microscope (Olympus, Japan) in triplicate for each group.

2.5. Immunohistochemical analysis

For immunohistochemistry, tissue samples were soaked in 3% hydrogen peroxide (H_2O_2) and methanol for 30 minutes to inactivate the endogenous peroxidase. The tissue slides were rinsed with PBS and then incubated with 3% bovine serum albumin to block nonspecific responses. The tissue sections were subsequently reacted with anti-desmin (1:200 dilution; rabbit polyclonal antibody; Abcam, UK) and anti-keratin 13 (1:50 dilution; mouse monoclonal antibody; ABIN126702) along with the secondary antibodies Alexa Fluor 488 goat anti-rabbit (ab150077; Abcam, UK) and Alexa Fluor 594 goat anti-mouse (ab150116; Abcam, USA), respectively. Desmin fluorescence was determined from the green-positive areas around the implanted site and quantified using the ImageJ software (n=5). The specifically expressed thickness (red color) of the regenerative esophageal epithelium was measured using the ruler tool of ImageJ software (n=5). Tissue sections for von Willebrand factor (vWF) (1:200 dilution; rabbit monoclonal antibody; Abcam, UK) and CD68 (1:100 dilution; mouse monoclonal antibody; Abcam, UK) were subsequently incubated using the horseradish peroxidase-conjugated kit (Vectastain®) and visualized using the chromogenic substrate 3,3' diaminobenzidine (DAB; Vector, pk-7800). Cell nuclei were counterstained with hematoxylin. Histological images were obtained using a fluorescence microscope (BX43-32FA1-S09; Olympus Optical, Tokyo, Japan). The numbers of vWF-positive vessels and CD68-positive cells were calculated using ImageJ. Five areas (200× magnification) were analyzed per slide (n = 5 per group) by a blinded observer.

2.5. Statistical analysis

The data are expressed as the means ± standard deviation. Statistical significance was determined via one-way analysis of variance (ANOVA) with Tukey-Kramer's post hoc test (GraphPad Prism 5, GraphPad Software, La Jolla, CA). Statistical significance was denoted as * ($P < 0.05$), ** ($P < 0.01$), and *** ($P < 0.001$).

Chapter 3. Results

3.1. Physical characteristics of the 3D-printed PCL patch

The structural morphology of the 3D-printed patches was analyzed using a scanning electron microscope. The results confirmed that the printed PCL strands were well layered on the substrate of the thin PCL film at the designed resolutions, as observed from the side view (Figure 3A). In addition, the diameter of each PCL strand of the lattice structure was approximately 300 ~ 400 μm (Figure 3B).

The mechanical properties of each type of patch sample (PCL-film patch, non-film patch, and TCN-loaded PCL-film patch) were examined by the tensile test (Figure 4-1). The results showed that the 3D-printed patch with PCL film statistically showed the highest tensile strength among the tested groups (Figure 4-2), whereas the antibiotic-loaded patches showed the lowest average tensile strength

3.2. Physical characteristics and antibiotic-releasing behavior of the antibiotic-loaded patch

The colors of antibiotic-loaded patches differed according to the loading concentration of TCN (Figure 5-1). Patches with higher loading concentrations of TCN appeared dark brown. The results of the *in vitro* mass analysis indicated that the patches with higher TCN concentrations had faster degradation rates (Figure 5-2A). In particular, the patch groups loaded with 2.5 mg showed significant mass reduction at all time points. In addition, it was confirmed that all groups (0.3, 1, and 2.5 mg concentration) exhibited sustained release through the release tests (Figure 5-2B). Particularly, the 0.3 mg TCN-loaded groups released almost all the loaded TCN within 30 days. However, the patch samples loaded with 1 mg and 2.5 mg TCN released approximately 60% and 43.2% of the TCN over 30 days, respectively. This result proves that a higher concentration of loaded drugs leads to longer release.

3.3. In vitro cytotoxicity tests of antibiotic-loaded PCL patches

In vitro cytotoxicity studies were carried out on PCL-film patches with and without TCN for comparison with Teflon as a positive control and latex as a negative control. From Figure 6A, it is evident that both the PCL-film patch and the PCL-film patch with 1% TCN exhibited outstanding biocompatibility with 100% MC3T3 cell viability in each assay. Furthermore, the cell viability rate was higher in the PCL-film patch with 1% TCN than in the PCL-film patch. This phenomenon was assumed to be the effect of an appropriate concentration (1%, w/w) of tetracycline that induced positive effects on the proliferation of MC3T3 cells and increased the optical density over the testing period [18]. The fluorescence of osteoblast cells in the presence of extractions from samples was pictured using dead/live staining (Figure 6B-E). Specifically, the latex group showed the lowest viability rate, with many dead cells visualized in Figure 6C. Meanwhile, the cells grew well in the PCL-film patch (Figure 6D) and the PCL-film patch w/ 1% TCN groups (Figure 6E). Overall, the in vitro cytotoxicity studies imply that all patch samples with and without loaded tetracycline were biocompatible and promoted cell proliferation compared with the control groups. These data indicate that our 3D printing fabrication of patches and tetracycline loading procedure promote cell viability and proliferation.

3.4. Outcomes of implanting the antibiotic-releasing patches in rat esophagus

All antibiotic-releasing patches were implanted in the artificial partial esophageal defects under microscopic view. Figure 7 shows the representative image of each esophageal patch implantation under the microscope. Most of the experimental rats survived but rapidly lost weight during the first week (Figure 8). However, their weight increased gradually and reached near their initial baseline weight by week 6. The non-TCN group showed significant differences in weight compared with the 3% TCN group from week 2. There was no significant weight difference among any of the groups with TCN-loaded patches. This is supposed to be due to the initial antibiotic effects. Whereas all rats in the defect group died by day 3.

Physical conditions were quantified by the animal's appearance and attitude scoring system (Figure 9). The 3% TCN group had a significantly increased appearance score at week 2 compared with the non-TCN patch group. The attitude score showed a significant difference between the non-TCN group and the 3% TCN group at both weeks 1 and 2. However, there was no difference in either parameter among all experimental groups from week 3 (data not shown). In terms of functionality, micro-CT analysis confirmed that no leak of oral injected contrast agent in the entire esophagus (Figure 10). No leaks were observed from the axial view of the area (dotted line) of the implanted site. These results prove that the esophageal mucosa was well-formed in all groups.

3.5. Culture and antimicrobial susceptibility test

We created an artificial fistula in the esophagus of all rats and conducted a bacteriological examination to detect the major microbiome. *Staphylococcus aureus* and *Streptococcus agalactiae* were detected in most rat models 3 days after the creation of the esophageal fistula (Table 2). Afterward, antimicrobial susceptibility testing was performed for these two bacteria (Table 3). *Staphylococcus aureus* and *Streptococcus agalactiae* were identified as resistant to benzylpenicillin and levofloxacin, respectively. However, they were sensitive to most other antibiotics. Of these, TCN was chosen as the target drug for this study.

We also analyzed the culture results of the patched group. On Day 3 after transplantation, bacteria were detected in both the non-TCN patch and 0.3-TCN patch groups at the transplanted areas. However, on Day 7, bacteria were detected in neither the TCN-loaded group but only in the non-TCN patch group. After 4 weeks, no bacterial specimens were found in cultures from any group.

3.6. Histology of the implanted site

H&E and Masson's trichrome staining were performed for the histological analysis of the implanted site (Figure 11-1~3). The rats in the control group exhibited a complete loss of the full thickness layer of the esophagus. However, there was no obvious inflammation observed in the groups containing antibiotics. At 4 weeks after transplantation, the partially injured epithelium under the graft was completely regenerated to form esophageal lumens in all patch groups. In addition, reconstruction of the submucous lamina propria under the implanted patch, represented in blue, was clearly observed in the TCN 1% and 3% groups. The blue color of Masson's trichrome staining is indicated by collagen deposition of the esophageal lamina propria. At week 12, gradual degradation of the 3D-printed PCL strands appeared, and the degraded area was filled with muscular layers. In particular, histological differences between each image demonstrated that higher concentrations of antibiotics resulted in faster degradation of PCL

3.7. Expression of M1/M2 macrophages

Figure 12 shows the expressions of M1/M2 macrophages in the periphery of the defect sites 4 weeks after transplantation. The rats in the control group exhibited the expression of M1/M2 macrophages 3 days after transplantation. M1 macrophages were strongly expressed in the non-TCN group (Figure 12-1). In particular, the number of CD-68 positive cells was significantly decreased in the TCN (3%) group compared with the TCN (0.3%) group (Figure 12-3A). These results prove that the antimicrobial activity in the defect area is maximized under an antibiotic concentration of 2.5 mg. In terms of tissue regeneration, the expression of M2 macrophages was significantly increased at the concentrations of 1% & 3%, compared with the rest of the patch groups (Figure 12-2 and 12-3B). This suggests that high concentrations of antibiotic patches have a definite effect on esophageal tissue regeneration.

3.8. Regeneration of muscular layer and epithelium

Regeneration of esophageal muscles along the 3D-printed pore structure was verified by desmin immunostaining (Figure 13-1). Muscle bundles penetrated between 3D-printed strands were strongly expressed in green. In particular, muscle regeneration was significantly improved in the TCN (1% and 3%) group compared with the other patch groups (Figure 13-2). The structural environment of the 3D-printed patch is believed to be effective for muscle regeneration. Regeneration of the esophageal mucosa at 12 weeks after transplantation was revealed by keratin-5 immunostaining (Figure 14-1). While the esophageal epithelium was broken in the defect group, all transplanted patch groups showed connectivity. Specifically, the thickness of the regenerated epithelium was significantly increased in all patch groups with or without antibiotics compared with the normal group (Figure 14-2). This result provides clear evidence that remodeling of stratified squamous epithelium is possible only by implantation of a naked 3D-printed patch layered with PCL film.

3.9. Analysis of neovascularization in the implanted sites

Immunostaining for the Von Willebrand factor (vWF) was performed to observe the neovascularization around each implanted patch (indicated in star; Figure 15-1). Newly formed vessels appeared in green near the implanted patch (inset box). As the loaded antibiotic concentrations increased, the number of newly formed blood vessels increased significantly (Figure 15-2). These results showed a positive effect on angiogenesis and tissue regeneration in environments that contained certain concentrations of antibiotics. The distribution of elastin fibers affecting the mechanical properties of the esophagus was analyzed by elastin staining (Figure 16). Particularly, histological degeneration had already begun in the defect group compared with the normal esophagus group. In contrast, elastin fibers were clearly observed in the antibiotic-loaded groups, and their structural morphology was similar to that of the normal group. Regeneration of the rich elastin component improves the physical properties of the esophagus, enabling esophageal peristalsis.

Chapter 4. Discussion

As mentioned in the introduction, no commercial artificial patch is available for pharyngoesophageal defects. Existing surgical patches are designed for use in aseptic conditions such as artificial blood vessels, abdominal walls, or dura mater. Therefore, if they are used in contaminated areas such as the digestive tract, they could lead to infection and loosening of the anastomosis site, which can cause leakage of the luminal site contents. The leakage can affect large vessels because of the anatomical specificity of the neck, and lead to life-threatening conditions such as carotid artery rupture or sepsis. To avoid such complications, despite the long operation times and donor site morbidity, flap surgery is usually preferred.[19] However if a patch is developed that can ensure rapid tissue regeneration and contamination resistance, the associated socio-economic losses can be reduced considerably.[12]

The patch used in this study was designed considering two concepts. The first was the adaptability to shear stress, and the second was the defense from leakage. The esophagus is continually stretched; therefore, tensile strength is an important characteristic in the reconstruction of the esophagus.[20] It is stretched not only in the lateral direction but also in the vertical direction for peristalsis. This is evident in the anatomical structure of the esophagus comprising circular and longitudinal muscles. We designed our patch with a lattice pattern to mimic this esophageal muscular structure and applied 3D printing technology for embodying this structure accurately.[21] While designing a

structure that can bear shear stresses, the lattice pattern was applied. The wide pore form in the lattice pattern was expected to provide a structured environment that is favorable for the penetration and regeneration of surrounding esophageal muscles. However, as the pores could cause leakage in the initial period of implantation, a thin film was interposed between the lattice patterns. Initially, we designed one lattice layer with one thin film, but stability was an issue. Finally, we designed the structure with one thin film between two lattice patterns, as shown in Figure 17. The 3D-printed PCL patch used in this study had structural advantages in pharyngoesophageal reconstruction.[12, 26]

For the proper selection of antibiotics, various bacteria extracted from the pus around the defect site were analyzed on Day 3 after the creation of the esophageal fistula. As listed in Table 2, *Staphylococcus aureu*s and *Streptococcus agalactiae* were mainly found in the esophageal fistulas. *Enterococcus faecalis*, *Staphylococcus Sciuri,* and *Escherichia coli* were excluded from the analysis, because they are a part of the normal flora and do not cause disease. TCN was selected as the target drug for the antibiotic susceptibility test for both *Staphylococcus aureus* and *Streptococcus agalactiae*. TCN is a well-known therapeutic drug as an anti-bacterial agent.[22, 23]

The hot-melting technique was used to uniformly distribute TCN in the biodegradable scaffolds.[24, 25] However, TCN molecules were incorporated between the PCL polymer chains, resulting in a loss of the polymer's inherent mechanical properties (Figure 5-2A and B). In addition, as the concentration of the loaded drug increases, the color of the scaffold becomes darker due to the

relative increase in TCN density in the printed PCL chains. Similarly, a faster degradation rate of the printed PCL scaffolds was observed with higher loading concentrations of TCN. Longer sustained-release periods were observed for the patch groups containing higher concentrations (2.5 mg) of TCN. In the group containing 1 mg TCN, approximately 60% of the TCN was released over 30 days, whereas, in the 2.5 mg group, only 43.2% of the TCN was released. It can be predicted from these results that a patch loaded with more than 1 mg TCN can exhibit sustained drug release for more than a month.

As the cascade of early infection, weakness of the anastomosis site, and contaminant leakage were some concerns, the anti-infection effect of antibiotic-releasing patches was considered a solution. One week after the surgery, the rats that had lost weight started regaining the weight in all patched groups (Figure 8). Additionally, there was no leakage sign in the μCT scan images obtained one month postoperatively. Furthermore, no leakage or bacterial infection was evident in the remaining interstitial tissue, in contrast with the control group, which exhibited continuous pus discharge or bacterial infection. This shows that the provision of just mechanical blockage can also have a significant effect on small defects. As mentioned in a previous paper, the pharynx and esophagus constitute a unique environment in which the luminal side is constantly surrounded by numerous bacteria. Therefore, the initial re-epithelialization of the defect site is of paramount importance.[21] In partial defects, the leakage blocking effect of the synthetic patch itself was adequate for initial re-epithelialization. However, histological analysis showed different results in each

group. Increasing concentrations of antibiotics were supplied by the patches, leading to the regeneration of the complete anatomic layers.

Interestingly, thick muscle layers were observed around the disassembled scaffolds by Masson's trichrome stain after 12 weeks (Figure 11-3). They were more prominent in Masson's trichrome stain at 4 weeks. For more precise evaluation, we conducted immunohistochemical analysis for desmin. Strong green fluorescence was observed around PCL strands. (Figure 13-1, indicated by stars) This showed that the 3D-printed strands had structural properties that facilitated muscle regeneration. A previous paper about the integrated design of 3D-printed tissue scaffolds had anticipated that wide pores in patches can provide a structured environment that is favorable for the penetration and regeneration of surrounding esophageal muscles.[27] Though muscle penetration was observed between PCL strands, it was not just the process of muscle regeneration. In the broad microscopic view, thick muscle layers were observed mainly under the patch. (Figure 11-3) Because of the patch size, the in-growing process of muscle regeneration might have been prioritized over the penetrating process. That the patch itself could have become a scaffold for the re-epithelialization process. The complete regeneration of the mucosal layer is essential not only for the formation of the mechanical barrier from the outside but also for the prospective regeneration of the submucosal and muscle layers.[28] Rapid regeneration of mucosal layers can be a firm foundation for the faster growth of muscle tissues beneath the patch.

In addition, sufficient ingrowth of blood vessels in the regenerated muscle and submucosa is essential for restoring the functional

properties of the esophagus.[29, 30] vWF staining showed significant vessel formation in the 1% and 3% TCN patch groups. In addition, the distribution and morphology of elastin, which is a measure of elasticity in the esophagus, were similar to that of the normal group in the patched groups with a high concentration of antibiotics. Adequate defense against bacterial insult during re-epithelialization can create a favorable environment for tissue regeneration.

The appearance of macrophages at Week 4 post-transplantation may provide important information in the support of this hypothesis. The expression of macrophages was significantly lower in the group treated with higher levels of antibiotics than in the groups with lower levels of antibiotics. In contrast, the expression of M2 macrophages, which are involved in tissue remodeling, was increased significantly in the 1% and 3% TCN groups compared with the 0.3% TCN group.

Recently, synthetic polymer scaffolds for pharyngoesophageal reconstruction have been actively studied because of their advantages of reproducibility, easy availability, xeno-free nature, and low cost. Moreover, various methods for reducing host reactions, such as mesenchymal stem cell seeding,[31] post-omental culture,[32] and smooth muscle seeding[33] have also been developed. However, no verified strategy can recreate a functional esophagus. To overcome the issue of pharyngoesophageal transplantation, the use of antibiotic-releasing surgical patches for antimicrobial activity and muscle tissue regeneration could be a favorable strategy.

Chapter 5. Conclusion

In the present study, an antibiotic-releasing patch with a 3D-printed lattice form and thin PCL film was developed as a novel pharyngoesophageal patch. We confirmed that TCN was successfully loaded into the patch in both the film and the 3D-printed layer with the lattice structure. *In vitro* analysis demonstrated the benefits of the antibiotic-releasing patch in supporting the sustained release of TCN, cell viability, and mechanical properties for esophageal implantation. TCN was proven to be effective against various bacterial insults *in vitro* and *in vivo* in this experimental setting. Our animal study using a partial esophageal defect rat model showed the importance of antibacterial activity in esophageal reconstruction. Among the test groups, the 1% and 3% TCN patches led to the most advanced esophageal regeneration, as identified by a thin layer of re-epithelialization, distinct muscle generation, and neovascularization, in the regenerative layer. Taken together, marked full-structural regeneration of the esophagus was observed with patches loaded with more than 0.3% concentration of antibiotics.

Newly designed 3D-printed antibiotic-releasing patches could be a promising biomaterial to treat infected wounds for advanced tissue regeneration. Our study results can help in the development of structures that can be applied in the reconstruction of diverse contaminated wounds. Furthermore, this study can guide the manufacture of patient-customized patches for different conditions by developing the technology to load various medicines in the patches,

Tables and Figures

Table 1. Appearance and Attitude Scales

Score	Appearance
5	Normal; normal skin tent and posture
4	Skin tent present on dorsum
3	Hunched posture, piloerection present, moderate skin tent
2	Eyes sunken in, piloerection and skin tent severe
1	Failure to right itself

Score	Attitude
5	Normal; active in cage prior to and during handing
4	Decreased activity, but alert, responsive to handling
3	Lethargic, decreased resistance to handing
2	Nonresponsive mouse only moves when touched
1	Failure to flee when hand is presented in cage

Table 2. pathogenic organisms isolated in esophageal swab

Microbe	Rats (model no.)									
	1	2	3	4	5	6	7	8	9	10
Stapylococcus aureus	+	+	+	+	+	+	+	+	+	+
Streptococcus pneumoniae	–	–	–	–	–	–	–	–	–	–
Streptococcus agalactiae	+	+	+	–	+	+	+	–	+	+
Beta strep. Grp G	–	–	–	–	–	–	–	–	–	–
Beta strep. Spp	–	–	–	–	–	–	–	–	–	–
Corynebacterium kutscheri	–	–	–	–	–	–	–	–	–	–
Salmonella spp.	–	–	–	–	–	–	–	–	–	–
lebsiella pneumoniae/oxytoca	–	–	–	–	–	–	–	–	–	–
Yersinia pseudotuberculosis	–	–	–	–	–	–	–	–	–	–
Citrobacter rodentium	–	–	–	–	–	–	–	–	–	–
Pseudomonas aeruginisa	–	–	–	–	–	+	–	+	–	–
Pasteurella pneumotropica	–	–	–	–	–	–	–	–	–	–
Pasteurella multocida	–	–	–	–	–	–	–	–	–	–
Bordetella bronchiseptica	–	–	–	–	–	–	–	–	–	–
Dermatophytes	–	–	–	–	–	–	–	–	–	–

Table 3. Antimicrobial susceptibility test results of representative organisms isolated in esophageal swab

Stapylococcus aureus			***Streptococcus agalactiae***		
Antimicrobial	**MIC[a]**	**Interpretation**	**Antimicrobial**	**MIC**	**Interpretation**
Cefoxitin Screen	NEG	-	Benzylpenicillin	<=0.06	S
Benzylpenicillin	>=0.5	R	Ampicillin	<=0.25	S
Oxacillin	0.5	S	Cefotaxime	<=0.12	S
Gentamicin	<=0.5	S	Ceftriaxone	<=0.12	S
Habekacin	<=1	S	Levofloxacin	>=16	R
Ciprofloxacin	<=0.5	S	Inducible Clindamycin Resistance	NEG	-
Inducible Clindamycin Resistance	NEG	-	Erythromycin	<=0.12	S
Quinupristin/Dalfopristin	<=0.25	S	Clindamycin	<=0.25	S
Erythromycin	<=0.25	S	Linezolid	<=2	S
Telithromycin	<=0.25	S	Vancomycin	0.5	S
Clindamycin	<=0.25	S	**Tetracycline**	<=0.25	S
Linezolid	2	S	Trimethoprim/ Sulfamethoxazole	<=10	S
Teicoplanin	<=0.5	S			
Vancomycin	1	S	-		
Tetracycline	<=1	S	-		
Tigecycline	<=0.12	S	-		
vancomycin	<=16	S	-		
Fusidic Acid	<=0.5	S	-		
Mupirocin	<=2	S	-		
Rifampicin	<=0.5	S	-		
Trimethoprim/ Sulfamethoxazole	<=10	S	-		

[MIC, Minimum inhibitory concentration; NEG, negative ; S, Susceptible; R, Resistant]
[a]The MIC of each agent is reported in micrograms per milliliter. The MIC was measured by broth dilution, and susceptibility or resistance was interpreted according to CLSI guidelines

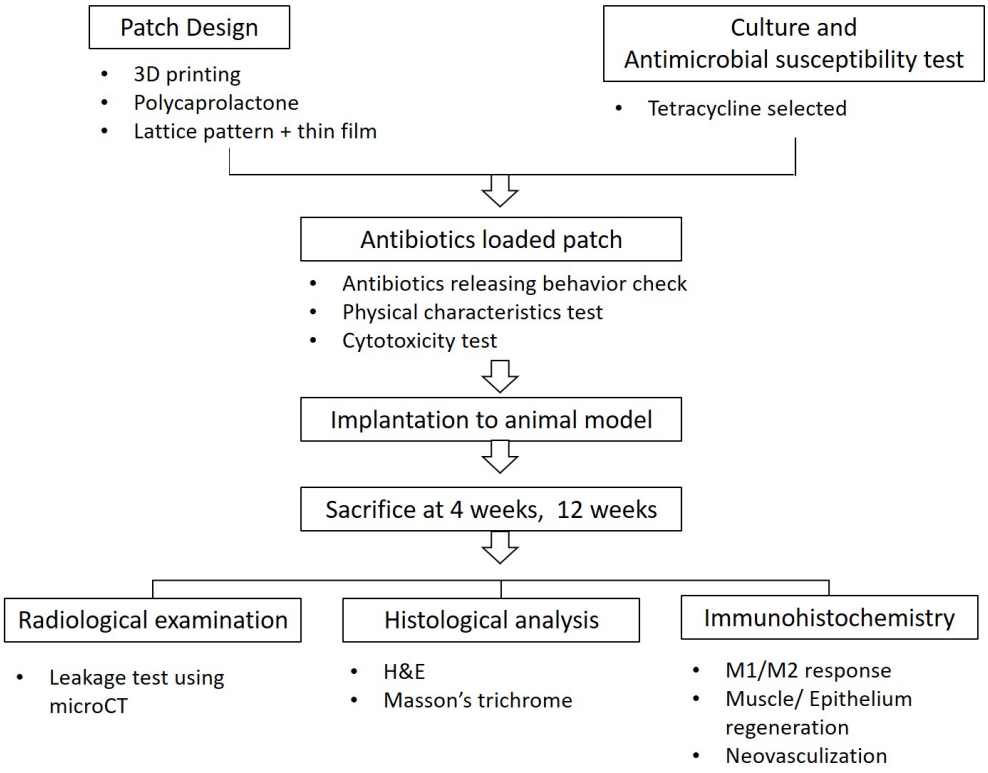

Figure 1.

Schematic flow chart of the study design.

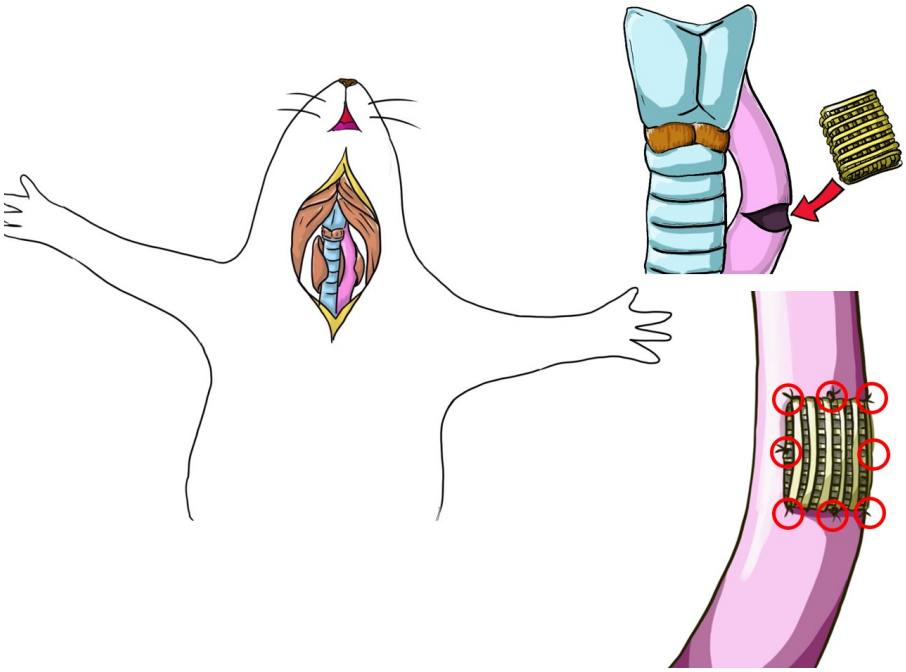

Figure 2. Schematic diagram of the surgery

Antibiotic-releasing polycaprolactone patches transplanted into partial esophageal defects in rats.
A 120° partial circumferential defect made in the esophagus of a rat, Then 8-way stitch performed under microscope (red circles).

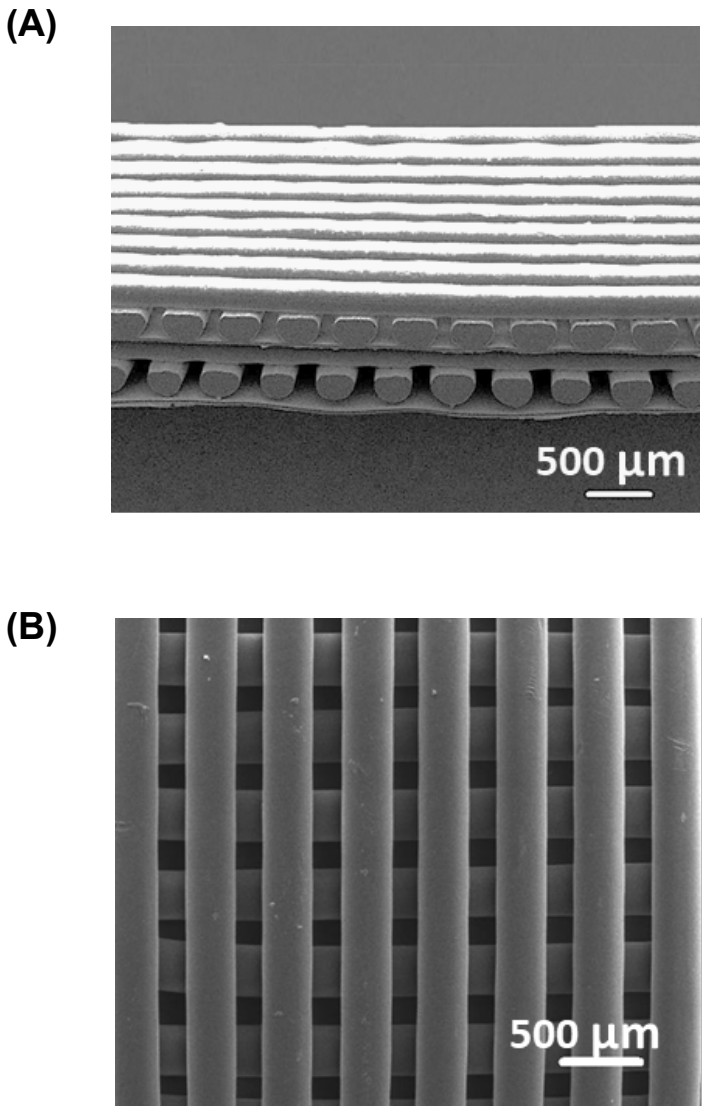

Figure 3.

Scanning electron microscope images of a polycaprolactone film patch with 1% tetracycline from (A) the side view and (B) the top view.

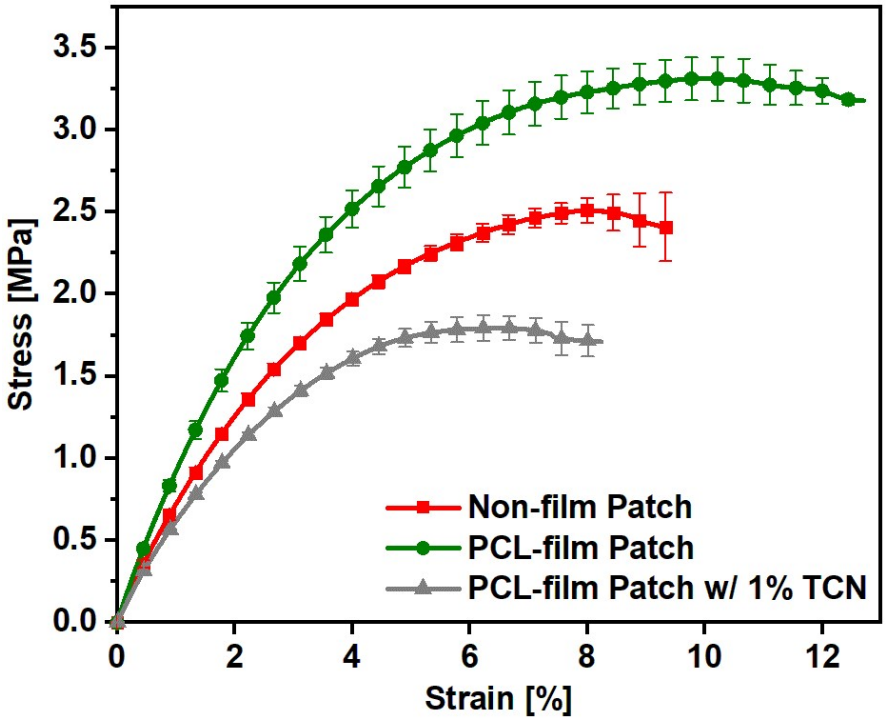

Figure 4-1.

Release profiles of the 3D-printed patches loaded with 0.3, 1 and 2.5 mg tetracycline in phosphate-buffered saline (pH 7.4) for 30 days at 37° C.

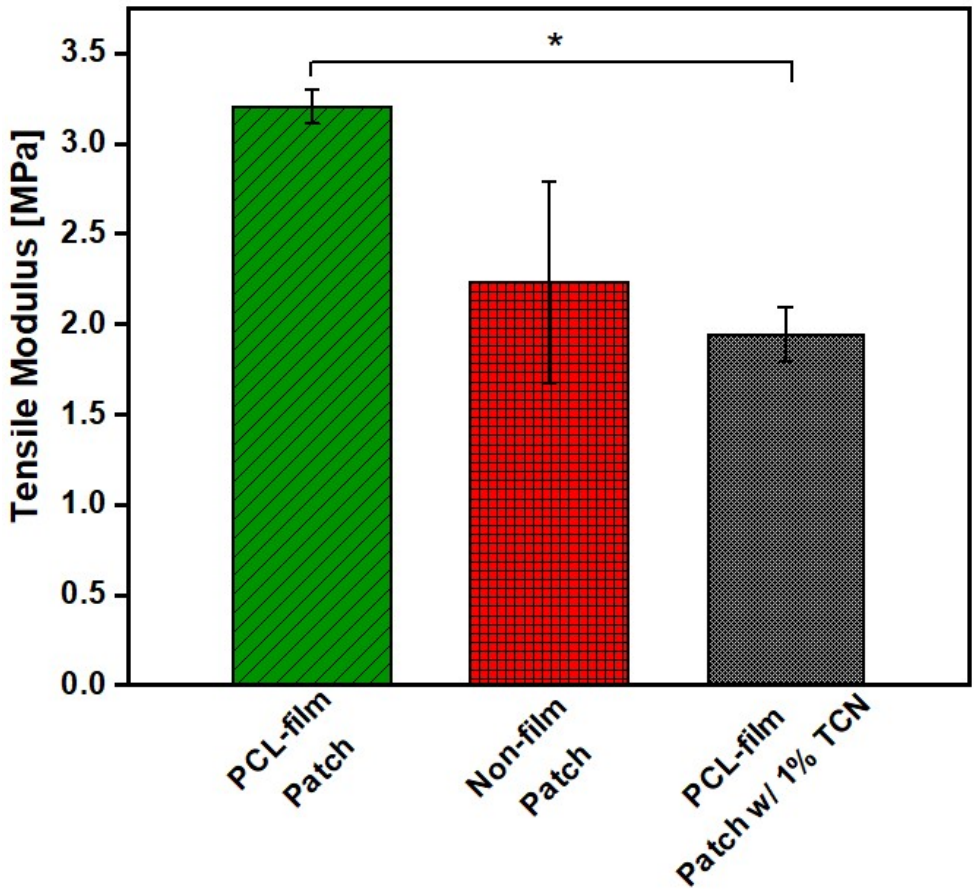

Figure 4-2.

Tensile modulus of the PCL-film patch, non-film patch, and PCL-film patch with 1% TCN (*p < 0.05)

PCL, polycaprolactone; TCN, tetracycline

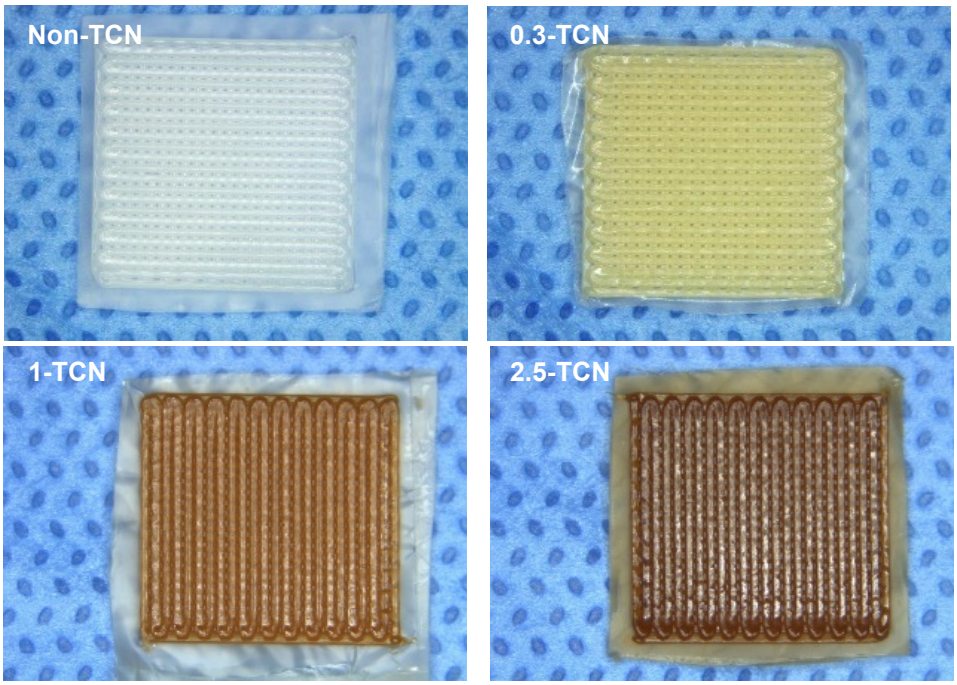

Figure 5-1.

Images of PCL-film patches loaded with different concentrations of TCN.

PCL, polycaprolactone; TCN, tetracycline

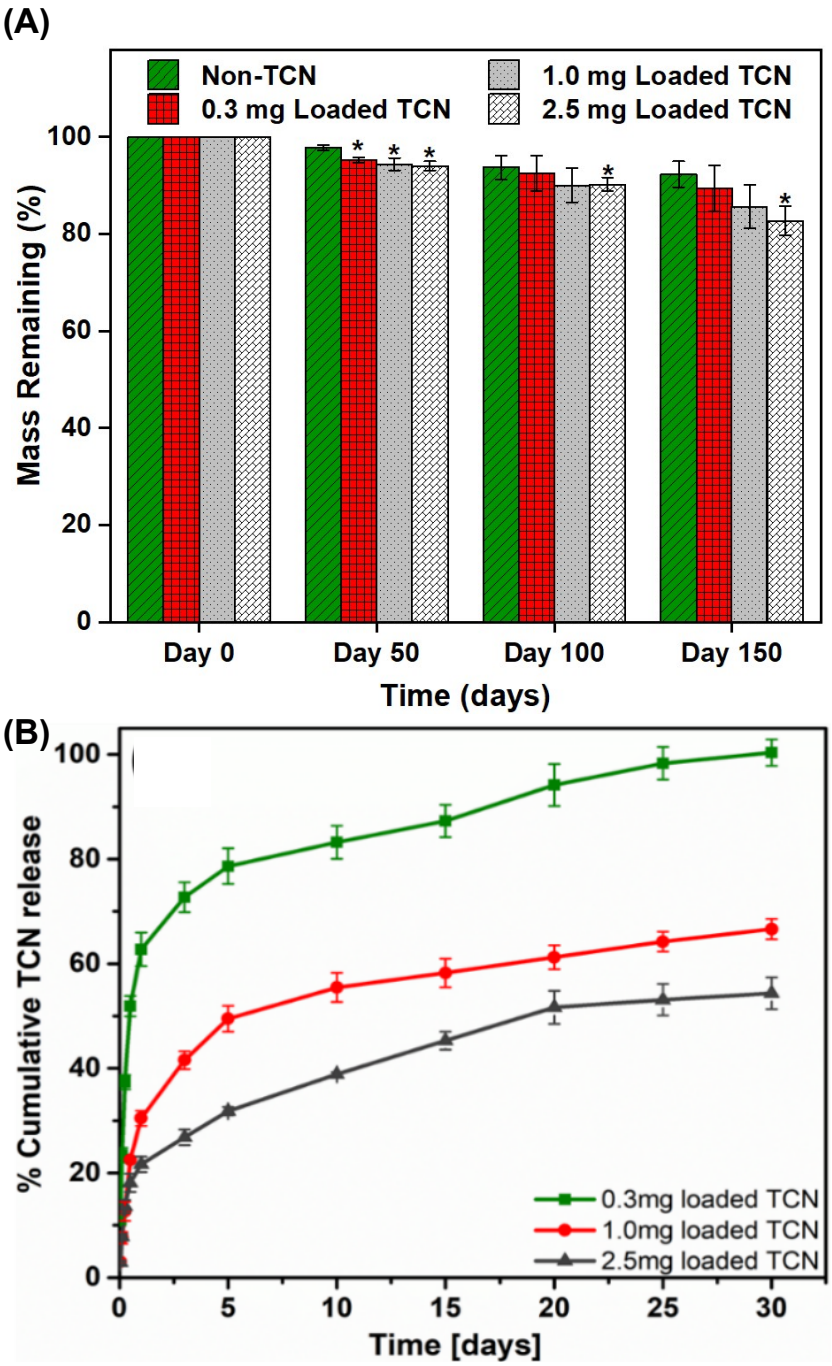

Figure 5-2.

(A) *in vitro* degradation rates

(B) Release profiles of the 3D-printed patches loaded with 0.3, 1 and 2.5 mg tetracycline (TCN) in phosphate-buffered saline (pH 7.4) for 30 days at 37° C.

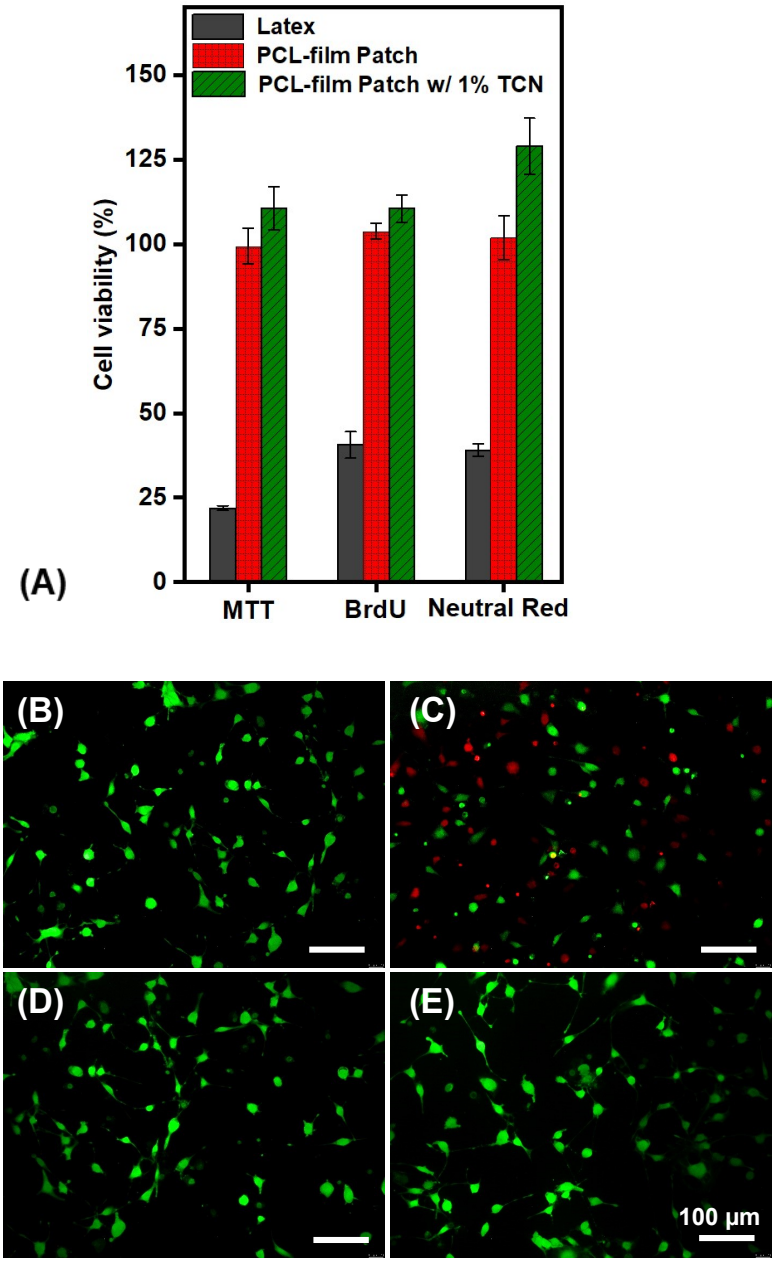

Figure 6.

(A) MC3T3 cell proliferation in the presence of extracts of Teflon, latex, PCL-film patch and, PCL-film patch with 1% TCN; Live/dead MC3T3 cells after the addition of extracts from (B) Teflon, (C) latex, (D) PCL-film patch and (E) PCL-film patch with 1% TCN after 3 days of in vitro cell culture. Live cells are stained green, while dead cells are stained red.

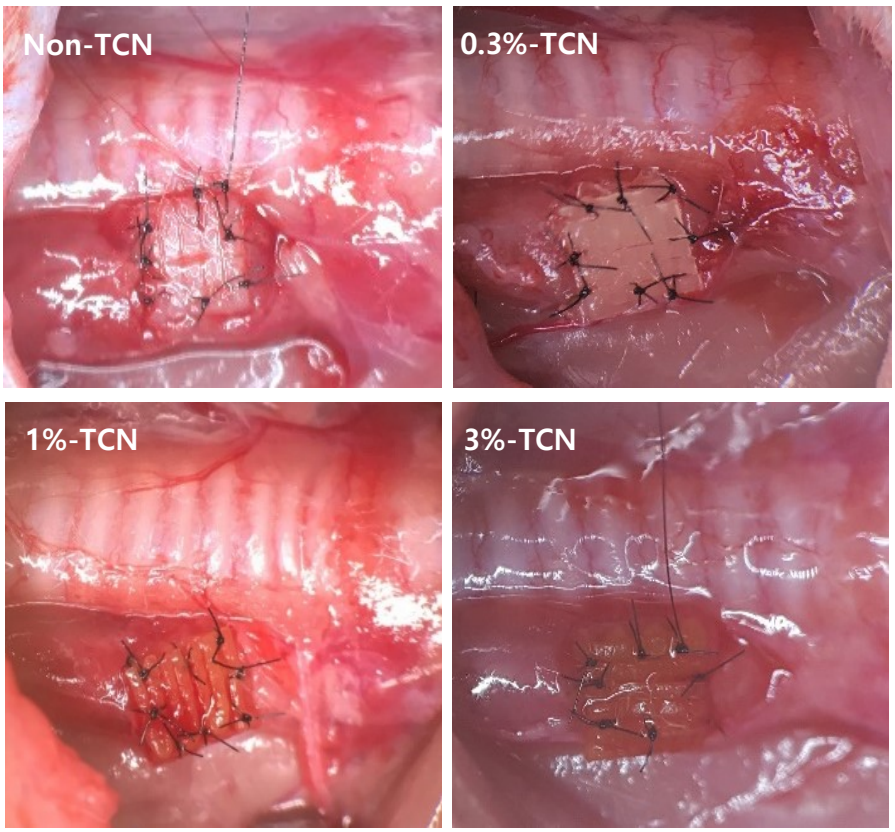

Figure 7.
Each antibiotic-releasing patch with or without TCN transplanted into full thickness esophageal defects in a rat model.

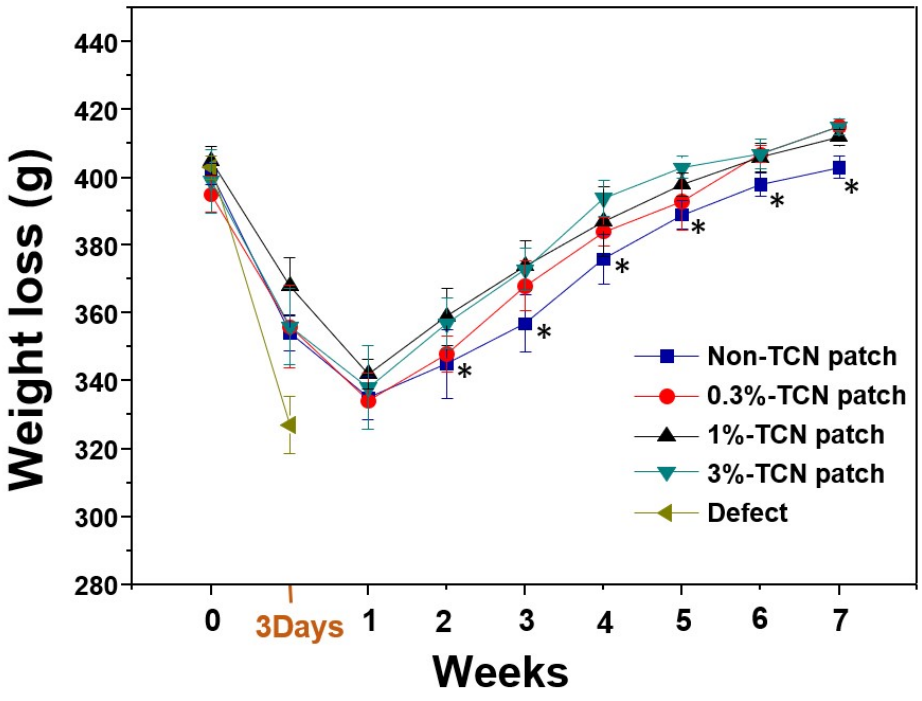

Figure 8.

Weight loss of the experimental animals in each group determined as absolute change from the initial weight.

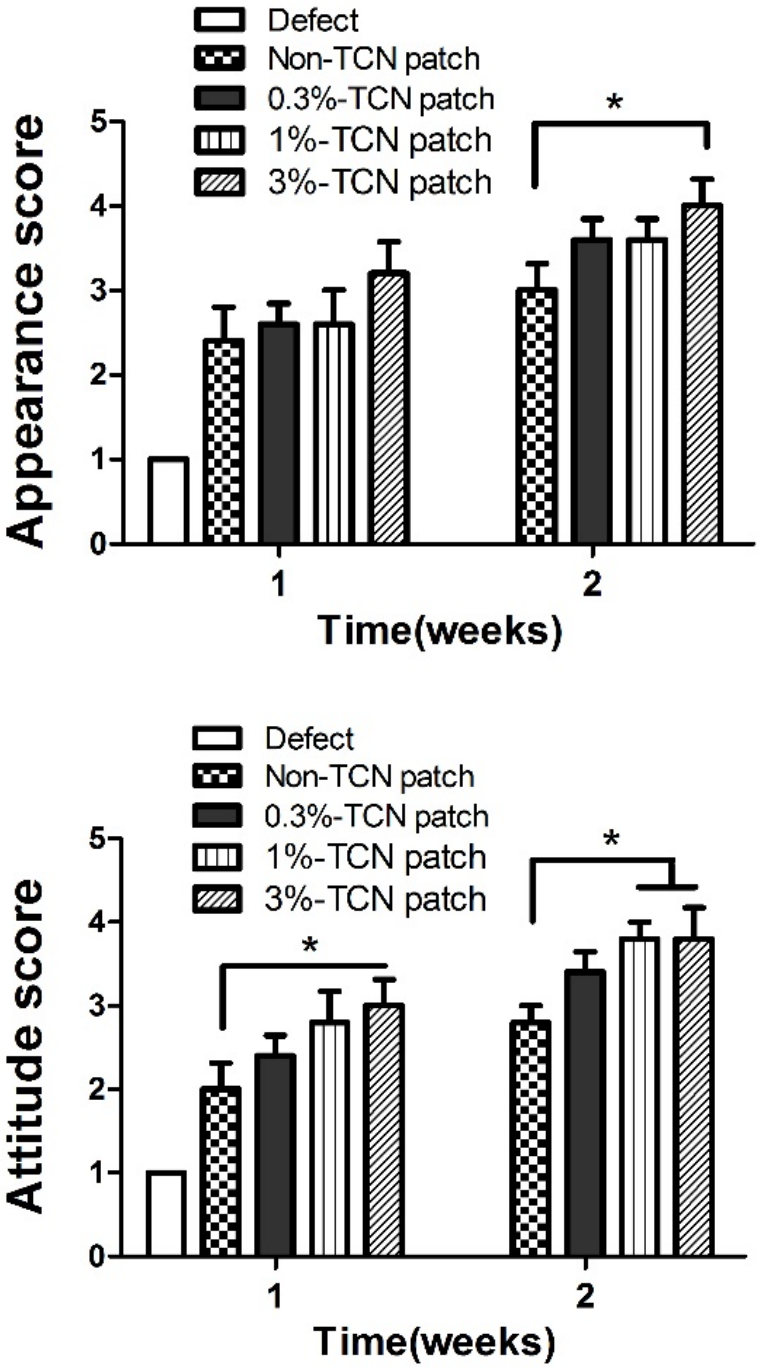

Figure 9.

Postoperative physical condition assessed using a score of behavior and appearance (*$p < 0.05$).

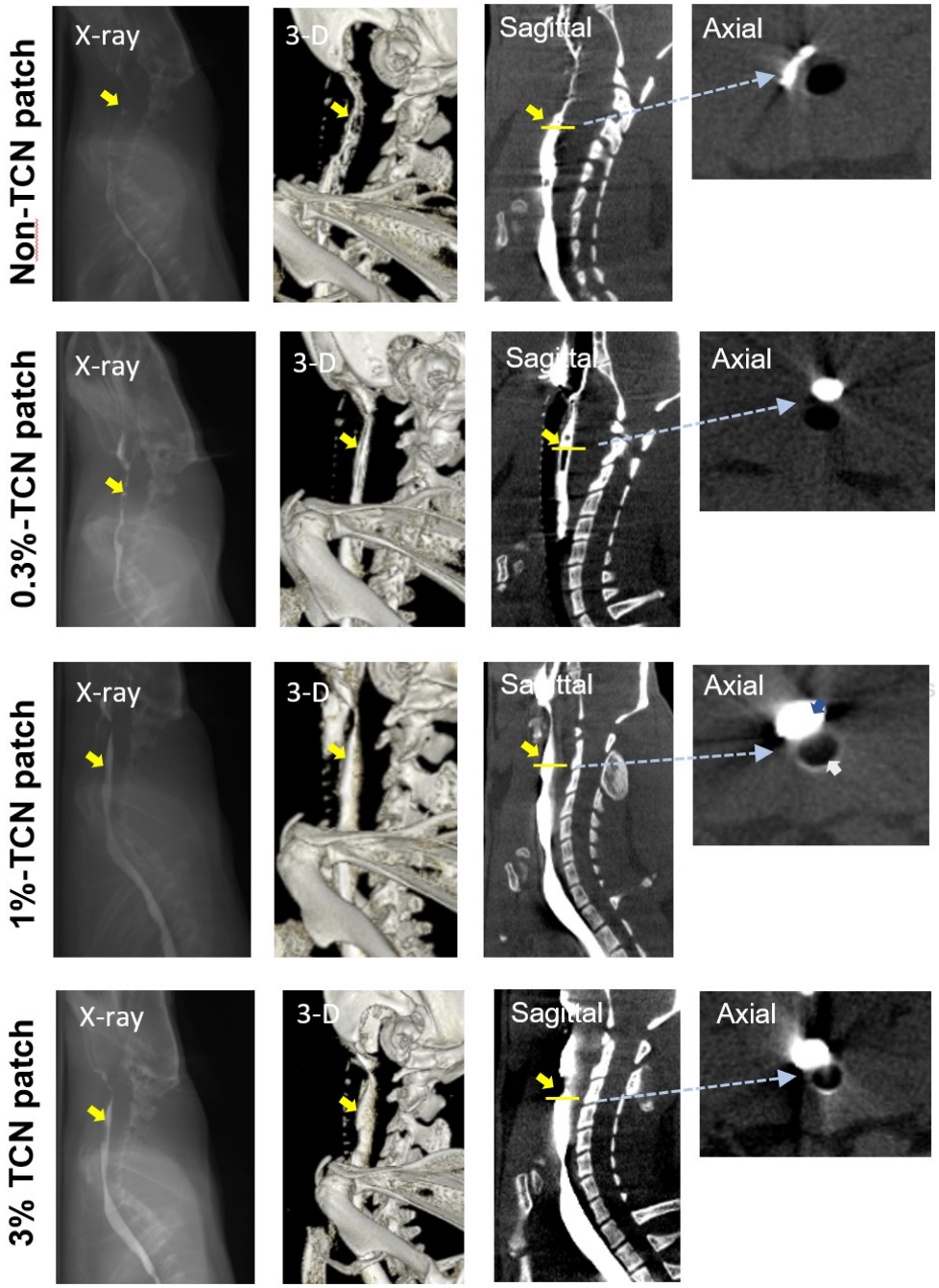

Figure 10.

Representative X-ray and micro-computed tomography images of the implanted site (yellow arrow) from each group.

Esophageal fistulas not observed in any of group.

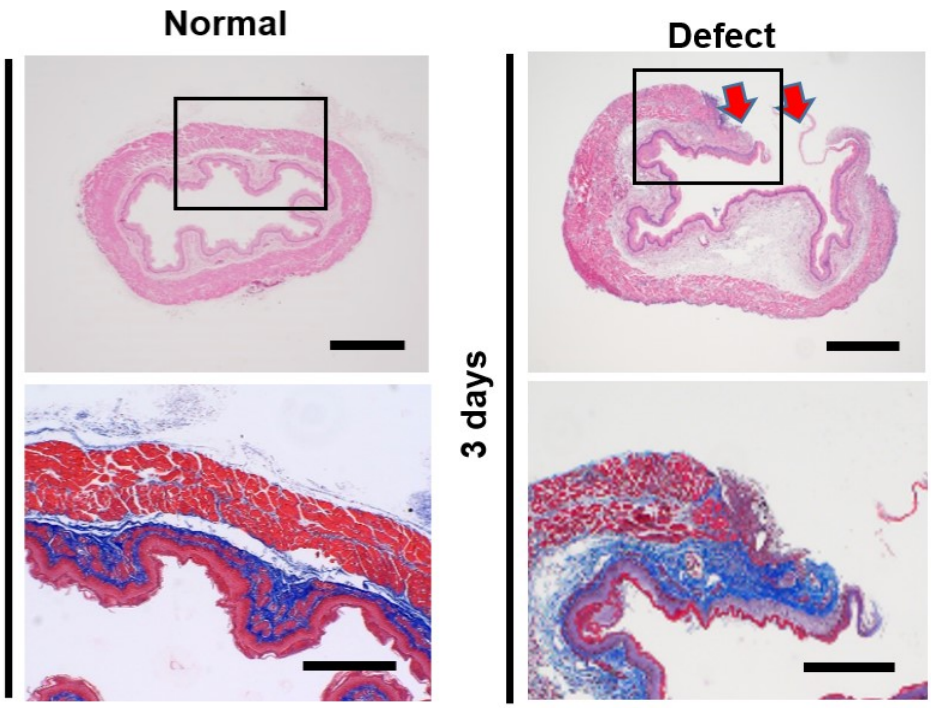

Figure 11-1. Normal and defect group

Histology of normal esophagus and defect only esophagus 3 days after implantation. Red arrows show artificial defect site.

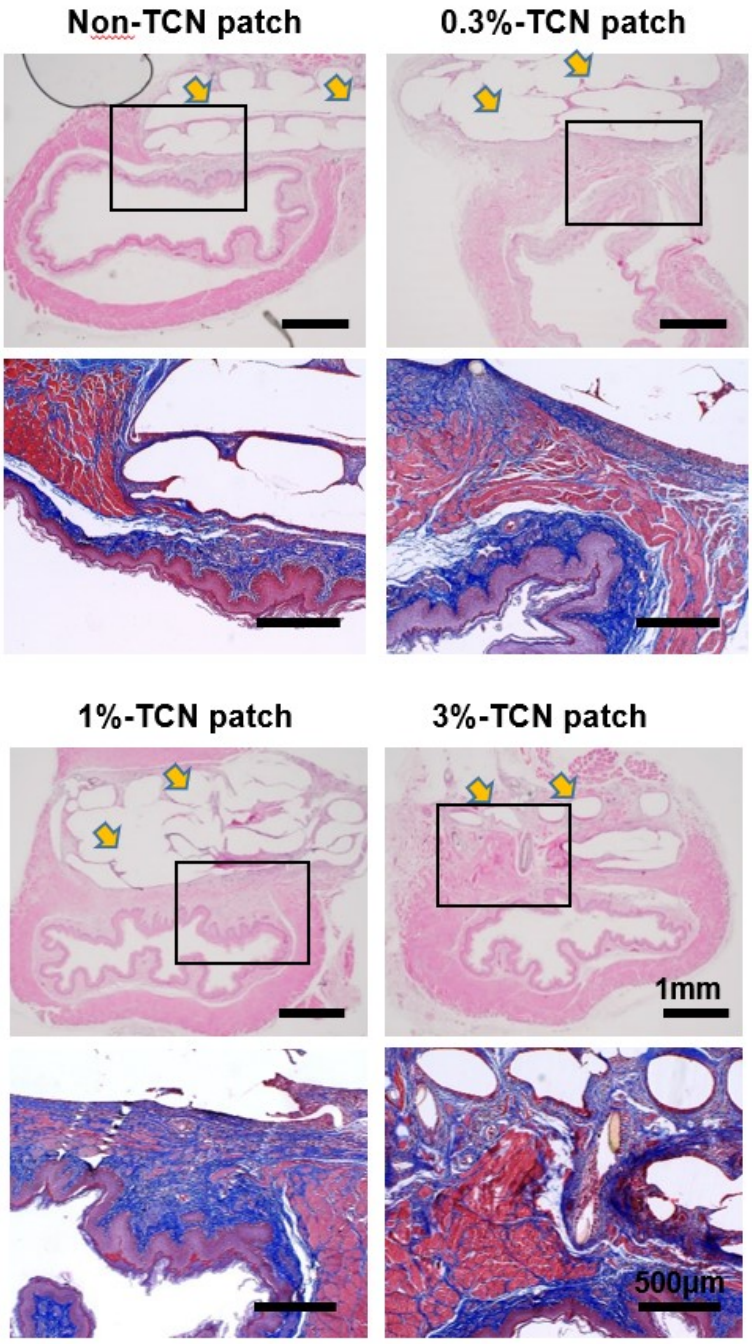

Figure 11-2. Postoperative Week 4

Histology of the reconstructed esophagus 4 weeks after implantation of patches with varied concentrations.

A newly formed epithelium can be seen beneath each implanted patch. (Yellow arrows indicate implanted patches.)

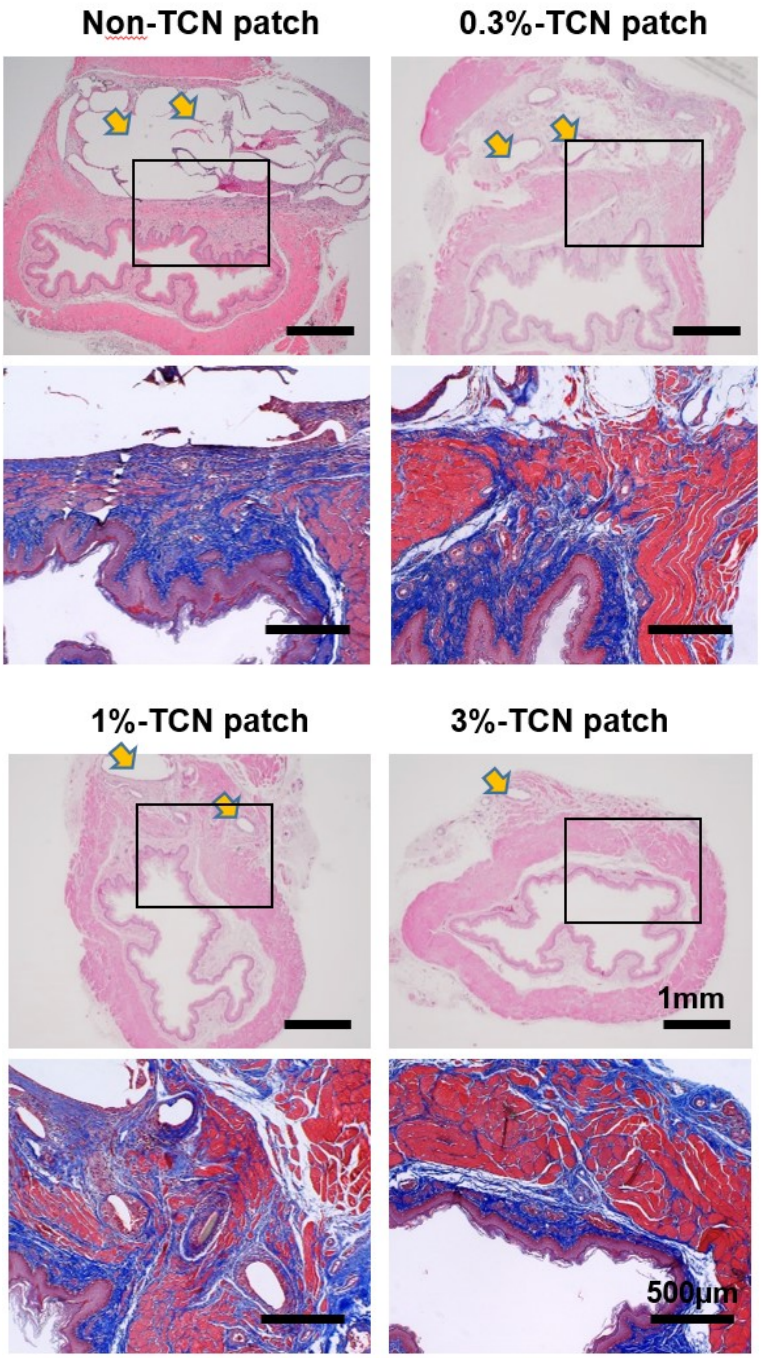

Figure 11-3. Postoperative Week 12

Histology of the reconstructed esophagus 12 weeks after implantation. Masson's trichrome stain showing collagen deposition (blue color) and muscle regeneration (red color) around the implanted sites in all group.

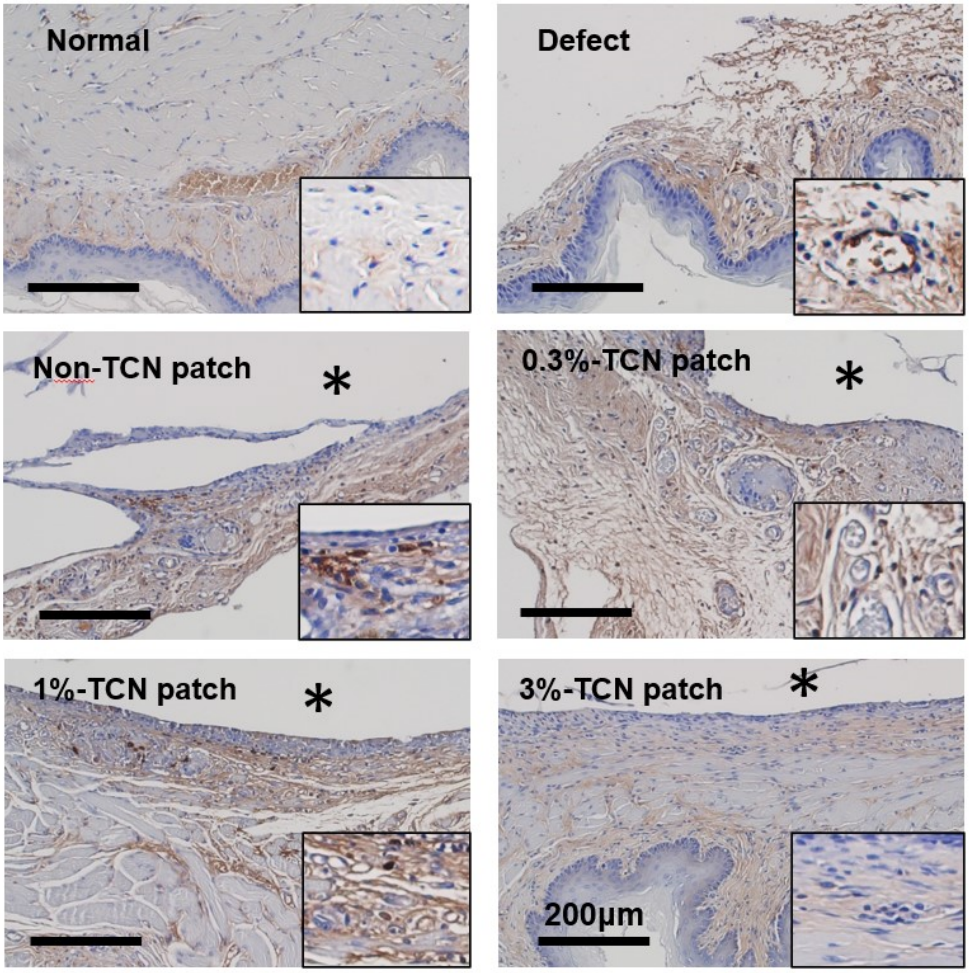

Figure 12-1. CD 68 immunostaining

Histological evaluation showing the distributions of M1 macrophages by CD68 immunostaining.

The brown dots indicate CD68-positive cells

(*, PCL strand).

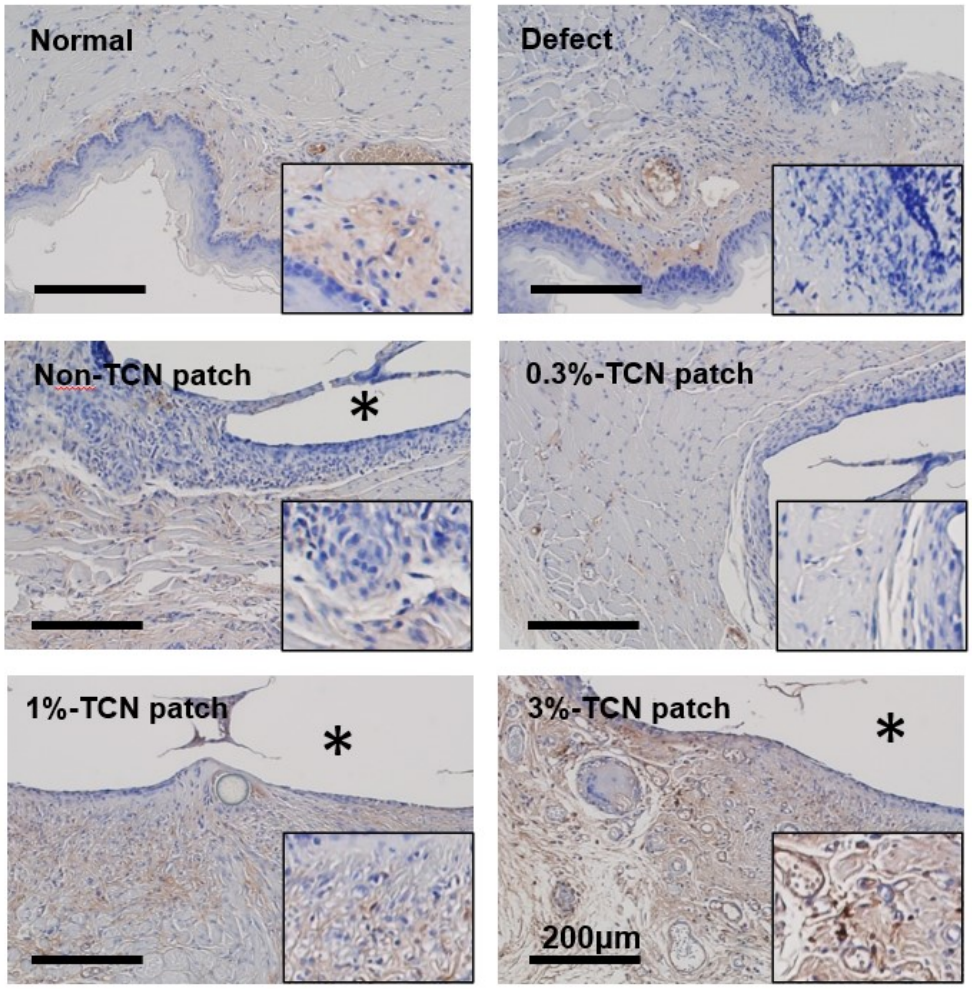

Figure 12-2. CD 163 immunostaining

M2 macrophage expression associated with tissue remodeling analyzed via CD163 immunostaining.

M2 macrophages strongly expressed in both the 1% and 3% TCN patch groups (brown color).

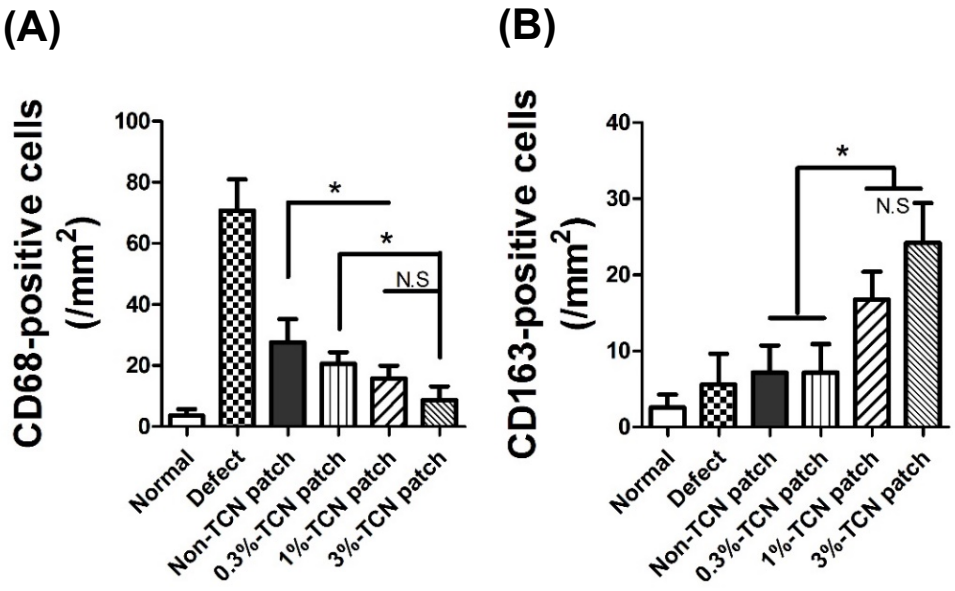

Figure 12-3.

Quantitative analysis of the number of CD68 / CD163 positive macrophages per square millimeter. In particular, M1 macrophage expression in the 3% TCN patch group was significantly lower than that in the 0.3% TCN patch group. Further, M2 macrophage expression in the 3% TCN patch group was significantly higher than that in the 0.3% TCN patch group.

(* $p < 0.05$)

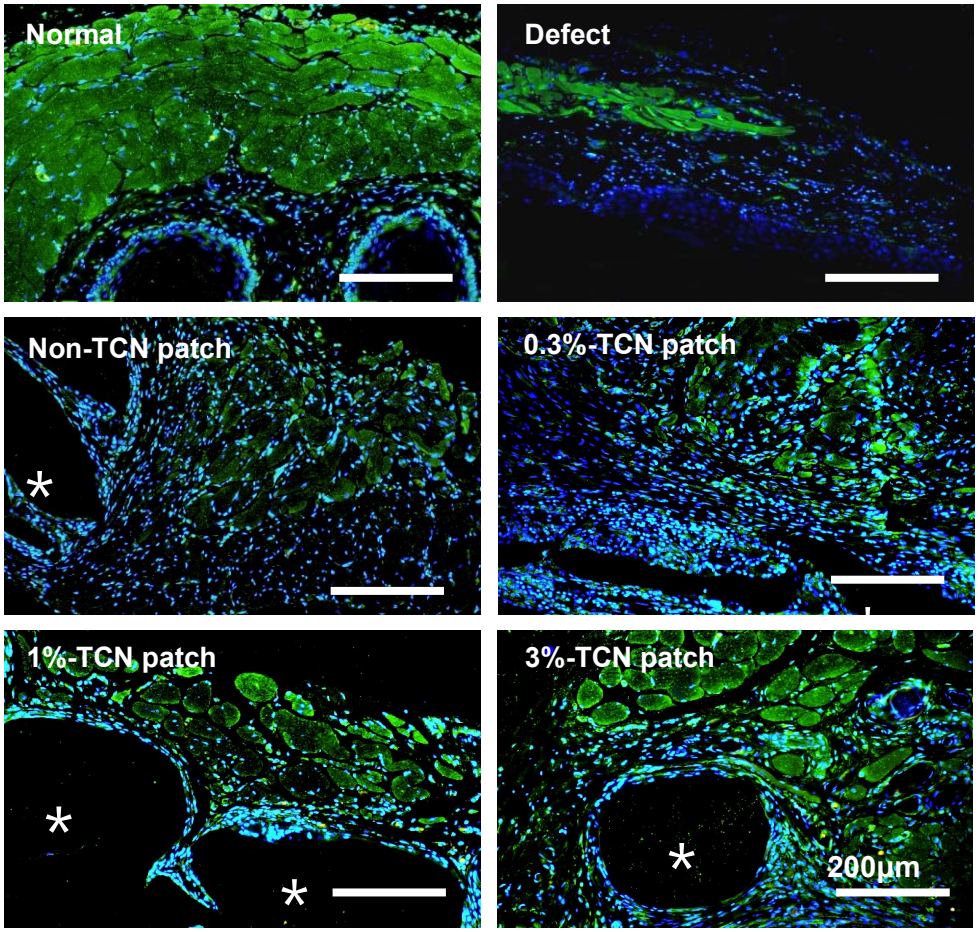

Figure 13-1.

Representative images of desmin-positive immunofluorescence in the reconstructed esophagus after transplantation. Desmin-positive signals showing newly regenerated muscle adjacent to the antibiotic-releasing patch (green color).

(*, 3D printing strand)

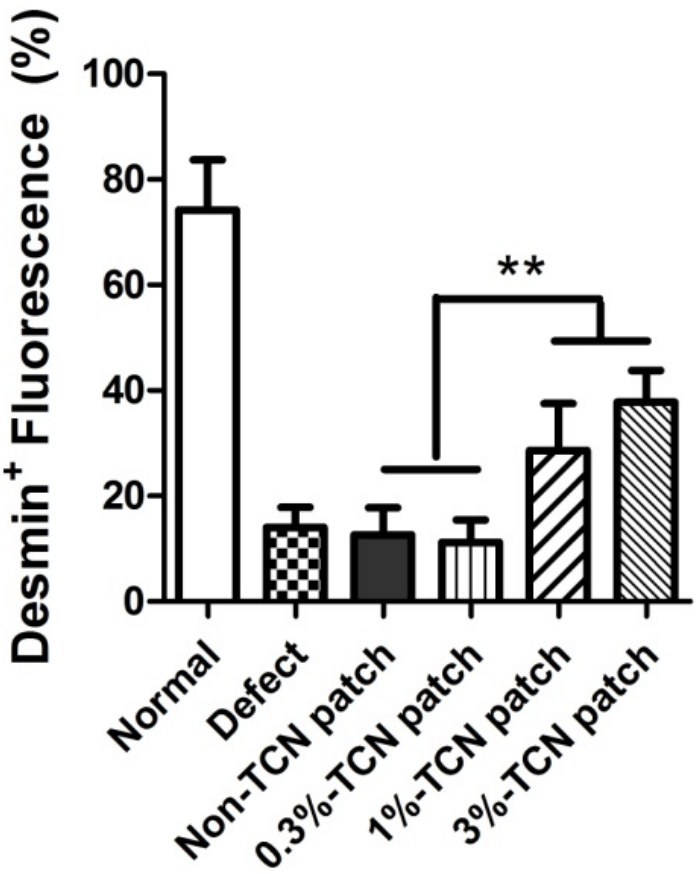

Figure 13-2.
Quantitative analysis of the desmin-positive area (**p<0.01).

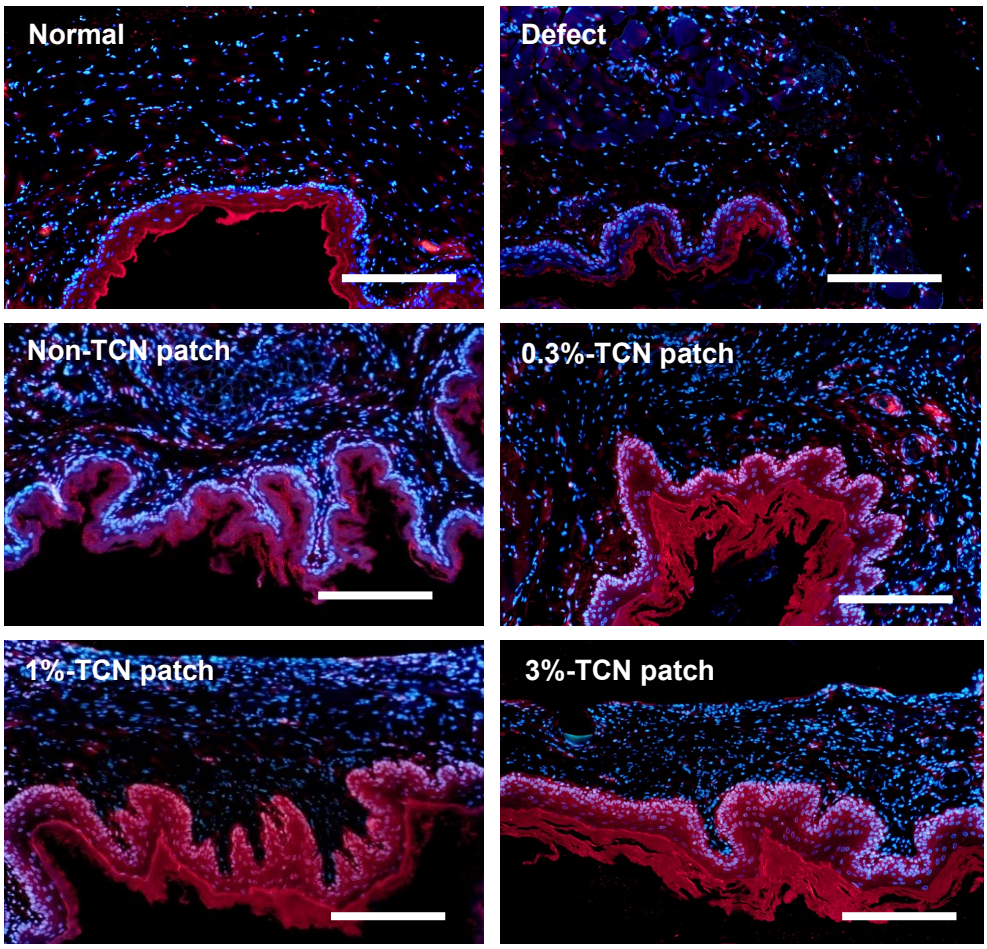

Figure 14-1.

Regeneration of esophageal mucosa at the implanted sites. Keratin-5 immunostaining showing newly formed epithelium 4 weeks after esophageal grafting (red color).

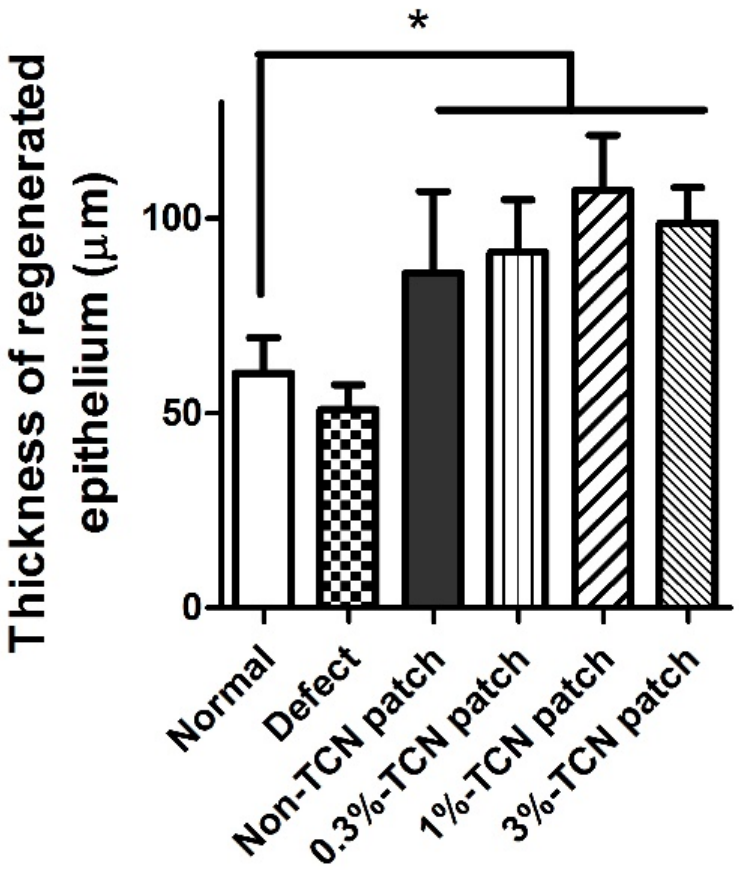

Figure 14-2.

Quantitative analysis of re-epithelialization 4 weeks after surgery (*p<0.05). All patch groups (with or without TCN) had a significantly thicker epithelial layers than the normal groups.

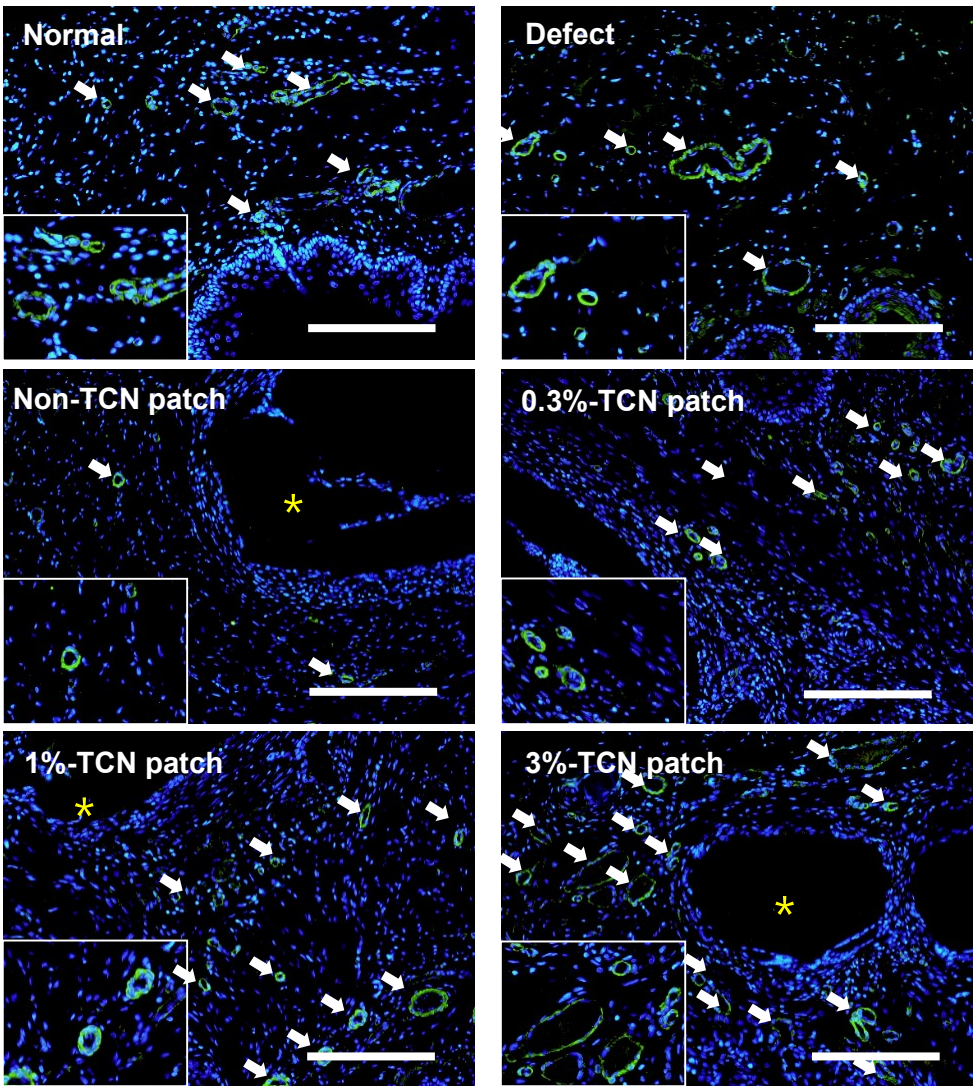

Figure 15-1.

Histological evaluation of neovascularization and elastin formation at 12 weeks after implantation.

Representative images showing the newly formed blood vessels by vWF expression. The arrows represent vWF-positive vessels. Inset boxes show magnified images of regenerated blood vessels (yellow star *, 3D-printed strand).

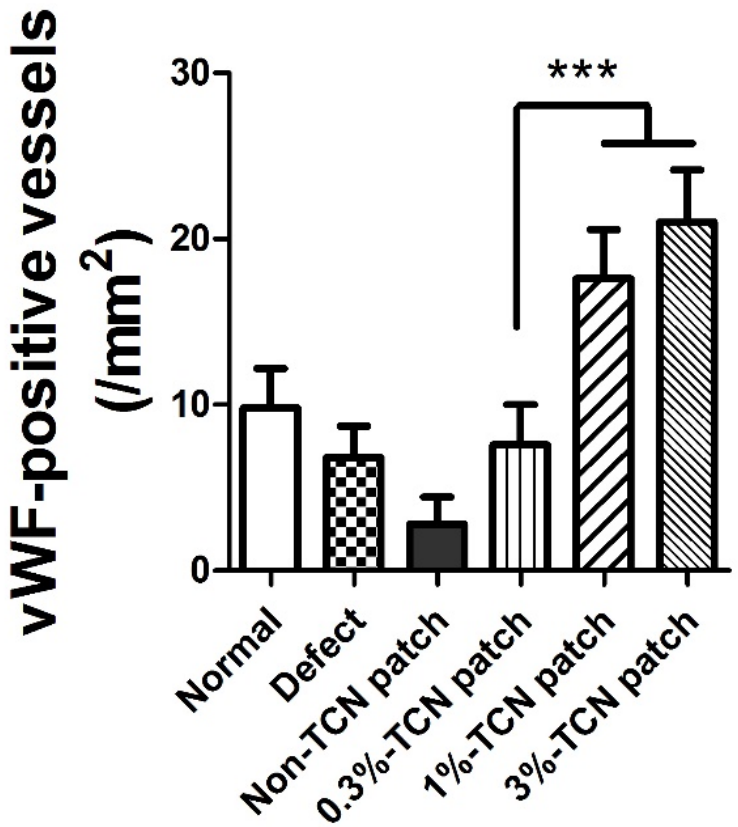

Figure 15-2.

Statistical analysis of the number of vWF-positive blood vessels per square millimeter.

vWF-positive vessel expression in the 3% TCN patch group was significantly higher than that in the 0.3% TCN patch groups.

(*** $p<0.001$)

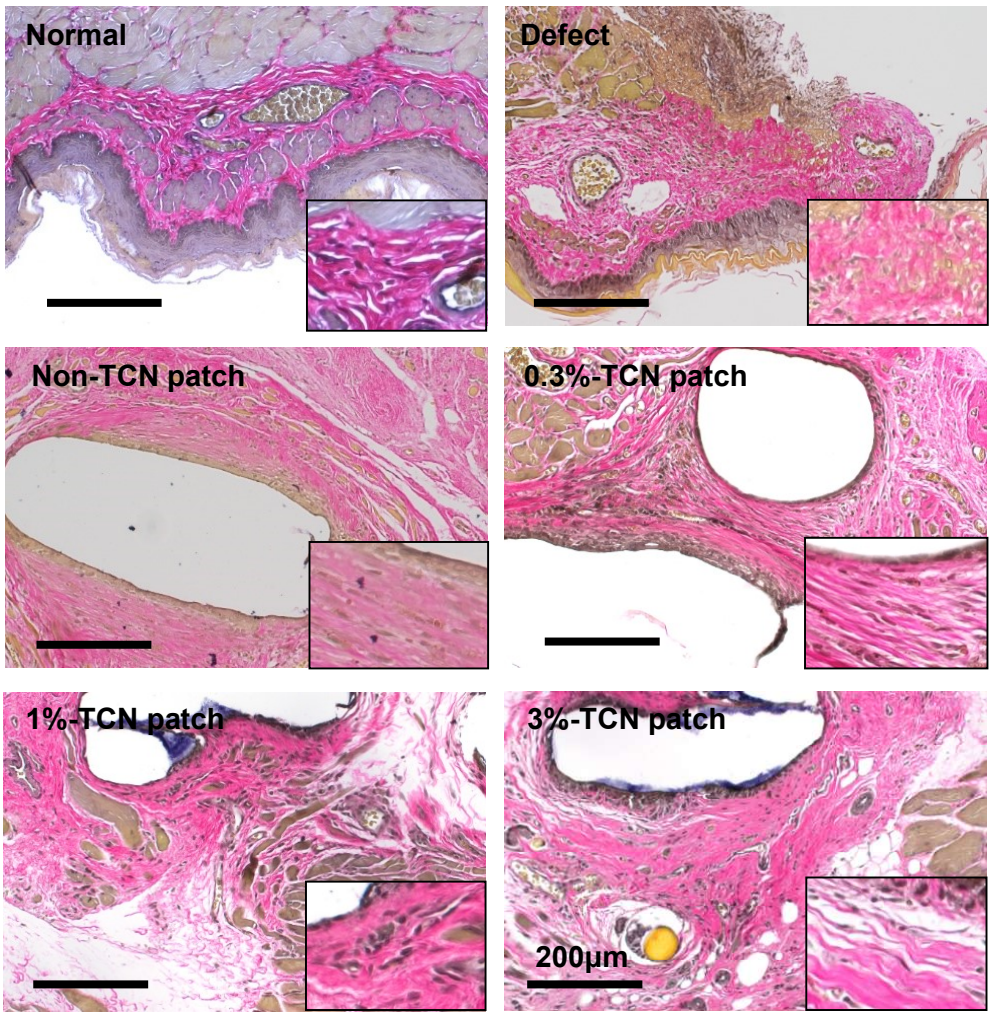

Figure 16.

Remodeling of elastin fiber, indicating the mechanical elasticity of the esophagus, investigated by elastin immunostaining. In all groups with antibiotic-loaded patches, a distinct morphology of elastin fibers can be seen compared with the non-TCN group.

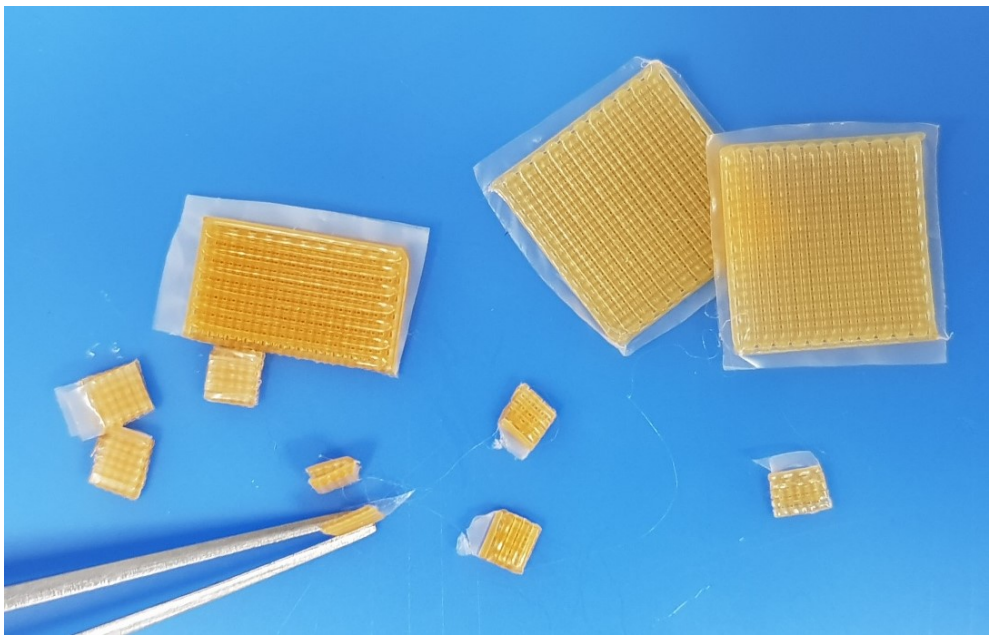

Figure 17.

Final manufactured form of the 3D-printed PCL patches.

A thin PCL film is seen between the 3D-printed PCL lattice patterns with 1 cm × 1 cm sized square shapes.

Bibliography

1. Norder Grusell, E., et al., Bacterial flora of the human oral cavity, and the upper and lower esophagus. Dis Esophagus, 2013. 26(1): p. 84-90.

2. Lerut, T., et al., Anastomotic complications after esophagectomy. Dig Surg, 2002. 19(2): p. 92-8.

3. Tabe, S., et al., Residual esophageal necrosis after radical esophagectomy for esophagogastric cancer: A case report. Mol Clin Oncol, 2020. 12(4): p. 321-324.

4. Kim Evans, K.F., et al., Esophagus and hypopharyngeal reconstruction. Semin Plast Surg, 2010. 24(2): p. 219-26.

5. Chen, H.C., et al., Microvascular prefabricated free skin flaps for esophageal reconstruction in difficult patients. Ann Thorac Surg, 1999. 67(4): p. 911-6.

6. Ki, S.H., J.H. Choi, and S.H. Sim, Reconstructive Trends in Post-Ablation Patients with Esophagus and Hypopharynx Defect. Arch Craniofac Surg, 2015. 16(3): p. 105-113.

7. Bakshi, A., D.J. Sugarbaker, and B.M. Burt, Alternative conduits for esophageal replacement. Ann Cardiothorac Surg, 2017. 6(2): p. 137-143.

8. Razdan, S.N., et al., Free Jejunal Flap for Pharyngoesophageal Reconstruction in Head and Neck Cancer

Patients: An Evaluation of Donor-Site Complications. J Reconstr Microsurg, 2015. 31(9): p. 643-6.

9. Zhan, K.Y., et al., Lymphoepithelial carcinoma of the major salivary glands: Predictors of survival in a non-endemic region. Oral Oncol, 2016. 52: p. 24-9.

10. O'Connell, D.A., et al., Swallowing function in patients with base of tongue cancers treated with primary surgery and reconstructed with a modified radial forearm free flap. Arch Otolaryngol Head Neck Surg, 2008. 134(8): p. 857-64.

11. Luc, G., et al., Decellularized and matured esophageal scaffold for circumferential esophagus replacement: Proof of concept in a pig model. Biomaterials, 2018. 175: p. 1-18.

12. Park, S.Y., et al., Tissue-engineered artificial oesophagus patch using three-dimensionally printed polycaprolactone with mesenchymal stem cells: a preliminary report. Interact Cardiovasc Thorac Surg, 2016. 22(6): p. 712-7.

13. Lee, J., et al., A desktop multi-material 3D bio-printing system with open-source hardware and software. International Journal of Precision Engineering and Manufacturing, 2017. 18(4): p. 605-612.

14. Das, D., et al., A terpolymeric hydrogel of hyaluronate-hydroxyethyl acrylate-gelatin methacryloyl with tunable properties as biomaterial. Carbohydr Polym, 2019. 207: p. 628-639.

15. Kim, I.G., et al., Tissue-Engineered Esophagus via

Bioreactor Cultivation for Circumferential Esophageal Reconstruction. Tissue Eng Part A, 2019. 25(21-22): p. 1478-1492.

16. Bang, S., et al., Evaluation of MC3T3 Cells Proliferation and Drug Release Study from Sodium Hyaluronate-1,4-butanediol Diglycidyl Ether Patterned Gel. Nanomaterials (Basel), 2017. 7(10).

17. Bekkevold, C.M., et al., Dehydration parameters and standards for laboratory mice. J Am Assoc Lab Anim Sci, 2013. 52(3): p. 233-9.

18. Yu, X., et al., Development of Biocompatible and Antibacterial Collagen Hydrogels via Dialdehyde Polysaccharide Modification and Tetracycline Hydrochloride Loading. Macromolecular Materials and Engineering, 2019. 304(5): p. 1800755.

19. Sartoris, A., et al., Reconstruction of the pharynx and cervical esophagus using ileocolic free autograft. Am J Surg, 1999. 178(4): p. 316-22.

20. Moschouris, K., N. Firoozi, and Y. Kang, The application of cell sheet engineering in the vascularization of tissue regeneration. Regen Med, 2016. 11(6): p. 559-70.

21. Chung, E.J., Bioartificial Esophagus: Where Are We Now? Adv Exp Med Biol, 2018. 1064: p. 313-332.

22. Carlborg, B., O. Densert, and C. Lindqvist, Tetracycline induced esophageal ulcers. a clinical and experimental study.

Laryngoscope, 1983. 93(2): p. 184-7.

23. Higuchi, D., et al., Etiology, treatment, and outcome of esophageal ulcers: a 10-year experience in an urban emergency hospital. J Gastrointest Surg, 2003. 7(7): p. 836-42.

24. Kotta, S., A. Nair, and N. Alsabeelah, 3D Printing Technology in Drug Delivery: Recent Progress and Application. Curr Pharm Des, 2018. 24(42): p. 5039-5048.

25. Tan, D.K., M. Maniruzzaman, and A. Nokhodchi, Advanced Pharmaceutical Applications of Hot-Melt Extrusion Coupled with Fused Deposition Modelling (FDM) 3D Printing for Personalised Drug Delivery. Pharmaceutics, 2018. 10(4).

26. Takeoka, Y., et al., Regeneration of esophagus using a scaffold-free biomimetic structure created with bio-three-dimensional printing. PLoS One, 2019. 14(3): p. e0211339.

27. Egan, P.F., Integrated Design Approaches for 3D Printed Tissue Scaffolds: Review and Outlook. Materials (Basel), 2019. 12(15).

28. Chung, E.J., et al., Development of an omentum-cultured oesophageal scaffold reinforced by a 3D-printed ring: feasibility of an in vivo bioreactor. Artif Cells Nanomed Biotechnol, 2018. 46(sup1): p. 885-895.

29. La Francesca, S., et al., Long-term regeneration and remodeling of the pig esophagus after circumferential resection using a retrievable synthetic scaffold carrying autologous cells. Sci

Rep, 2018. 8(1): p. 4123.

30. Nieponice, A., et al., Patch esophagoplasty: esophageal reconstruction using biologic scaffolds. Ann Thorac Surg, 2014. 97(1): p. 283-8.

31. Lee, D.Y., et al., Synergistic effect of laminin and mesenchymal stem cells on tracheal mucosal regeneration. Biomaterials, 2015. 44: p. 134-42.

32. Grikscheit, T., et al., Tissue-engineered esophagus: experimental substitution by onlay patch or interposition. J Thorac Cardiovasc Surg, 2003. 126(2): p. 537-44.

33. Nakase, Y., et al., Intrathoracic esophageal replacement by in situ tissue-engineered esophagus. J Thorac Cardiovasc Surg, 2008. 136(4): p. 850-9.

Abstract

3D 프린팅을 이용한 항생제 방출 식도 패치의 조직 재생 효과에 대한 연구

성 명 : 김 성 동
학과 및 전공 : 의학과 이비인후과학 전공
서울대학교 대학원

식도 결손은 결손부에 대한 다양한 세균총에 대한 노출을 유발하며, 이는 심한 염증 반응을 유발한다고 알려져 있다. 저자 및 연구진은 생분해성 polycaprolactone (PCL)을 사용하여 3D 프린터로 격자 모양 및 박막으로 구성된 패치를 제작하였고, 여기에 항생제, tetracycline (TCN)이 방출될 수 있도록 하여 인공적으로 만든 식도 결손에 대한 재건을 시도하였다. 이후 정성적, 정량적 분석을 통해 패치의 활용도와 효능을 평가하였다.

PCL은 미리 작업된 박막 위에 100 μm 해상도의 격자 모양으로 3D 프린팅 하였으며, 100° C에서 녹인 TCN와 PCL 입자를 혼합하여 3D 프린팅 함으로써 TCN이 패치에서 방출될 수 있도록 하였다. 체외실험에서 TCN 은 1달 이상 지속적으로 방출되는 것을 확인할 수 있었으며, 또한 세포독성에 대한 체외실험에서 패치 추출물이 뛰어난 세포적합성을 보임을 확인할 수 있었다. 이후 쥐에서 부분 식도결손을 유발한 후 제작된 패치를 적용하였고 3주 후 micro CT를 이용해 누출 여부를 확인하였다. 쥐의 구강을 통해 조영제를 주사하여 확인한 결과 모든 패치 이식군에서 식도 전장에 누출은 관찰되지 않았다. 수술 후

4주 및 12주에 각각의 군을 희생하여 조직학적 재생 정도를 확인한 결과, 1% 와 3% TCN 패치 그룹에서 유의미한 근육층 재생이 관찰되었고, 면역조직화학염색 분석 결과, 1% 및 3% TCN 패치 그룹에서 재 상피화 및 이식부위 주변 신생혈관 생성이 잘 이루어진 것을 확인할 수 있었다.

본 연구에서는 3D 프린팅을 이용한 항생제 방출 패치를 활용하였을 때, TCN의 항균 효과와 더불어 누공 주위에 식도 근육층을 비롯한 조직 재생에도 충분한 효과가 있음을 확인하였으며 이는 추후의 연구에서 매우 활용성이 높을 것으로 생각된다.

Keywords : 식도, 재건, 조직공학, 외과적 패치, 항생제 방출 패치
Student Number : 2018-31720